and variations of it have been studied by Stutt and Spafford [32], Spafford [33], and Rummler [34]. We suggest that the reader consult these references, because they provide an excellent demonstration of how the doubly-spread reverberation model of this section can be used to obtain effective practical systems. Various facets of the question are developed in the problems (e.g., Problems 13.2.17 and 13.2.18).

This completes our discussion of the reverberation and clutter problem. We now turn to a different type of problem.

13.3   DETECTION OF DOUBLY-SPREAD TARGETS AND COMMUNICATION OVER DOUBLY-SPREAD CHANNELS

In this section we consider two closely related problems. The first problem arises in the radar and sonar area and consists of trying to detect the return from a doubly-spread target in the presence of additive noise. The second problem consists of communicating digital data over a doubly-spread channel.

The section is divided into four parts. In Section 13.3.1, we formulate the quantitative models for the two problems and derive expressions for the optimum receivers and their performance. The results contain integral equations or differential equations that cannot be solved exactly in most cases. In Section 13.3.2, we develop approximate target and channel models that enable us to obtain a complete solution for the optimum receivers and their performance. In Section 13.3.3, we calculate the performance of a particular binary communication scheme to illustrate the techniques involved. In Section 13.3.4, we discuss some related topics.

13.3.1   Problem Formulation

In this section we formulate the detection and binary communication problem quantitatively.

13.3.1.A.   Detection. The first problem of interest is the radar or sonar detection problem. We transmit a signal whose complex envelope is $\sqrt{E_t}\tilde{f}(t)$. If a doubly-spread target is present, the complex envelope of the returned signal is

$$\tilde{s}(t) = \int_{-\infty}^{\infty} \sqrt{E_t}\tilde{f}(t-\lambda)\tilde{b}(t,\lambda)\,d\lambda, \tag{142}$$

where $\tilde{b}(t,\lambda)$ is a sample function from a complex Gaussian process whose covariance function is given in (37). We are using the process defined in (36), but the subscript x is omitted. The covariance function of $\tilde{s}(t)$ is

given by (22) as

$$\tilde{K}_{\tilde{s}}(t, u) = E_t \int_{-\infty}^{\infty} \tilde{f}(t - \lambda) \tilde{K}_{DR}(t - u, \lambda) \tilde{f}^*(u - \lambda) \, d\lambda. \tag{143}$$

In addition to the signal component, the received waveform contains an additive complex white noise $\tilde{w}(t)$, whose covariance function is

$$E[\tilde{w}(t)\tilde{w}^*(u)] = N_0 \, \delta(t - u). \tag{144}$$

The received waveform is just the noise term, $\tilde{w}(t)$, if the target is not present. Thus, we have a binary hypothesis testing problem in which the received complex envelopes on the two hypotheses are

$$\tilde{r}(t) = \tilde{s}(t) + \tilde{w}(t), \qquad T_i \le t \le T_f : H_1, \tag{145}$$

$$\tilde{r}(t) = \tilde{w}(t), \qquad T_i \le t \le T_f : H_0. \tag{146}$$

On both hypotheses, $\tilde{r}(t)$ is a sample function of a complex Gaussian random process. If we compare (145) and (146) with the equations specifying the detection problem in Chapter 11 [(11.30) and (11.31)], we see that the form is identical. The only difference is in the form of the covariance functions of the signal processes. Therefore all of the results in Chapter 11 that contain $\tilde{K}_{\tilde{s}}(t, u)$ as an arbitrary covariance function are valid for the problem of current interest. Specifically, (11.33)–(11.40) and Figs. 11.7–11.9 are valid relations for the receiver structures, and (11.50)–(11.54) are valid expressions for the performance. It is when we evaluate these various formulas that the doubly-spread model becomes important. Specifically, we shall find that the covariance function given in (143) is harder to work with than the covariance functions encountered in the singly-spread cases.

Some of the pertinent results from Chapter 11 are listed for ease of reference. The likelihood ratio test is

$$l_R = \frac{1}{N_0} \int_{T_i}^{T_f} \tilde{r}^*(t) \tilde{h}(t, u) \tilde{r}(u) \, dt \, du \underset{H_0}{\overset{H_1}{\gtrless}} \gamma, \tag{147}$$

where $\tilde{h}(t, u)$ satisfies the integral equation

$$N_0 \tilde{h}(t, u) + \int_{T_i}^{T_f} \tilde{h}(t, z) \tilde{K}_{\tilde{s}}(z, u) \, dz = \tilde{K}_{\tilde{s}}(t, u), \qquad T_i \le t, u \le T_f, \tag{148}$$

and $\tilde{K}_{\tilde{s}}(t, u)$ is given in (143). The estimator-correlator realization is shown in Fig. 11.7.

An alternative expression for the likelihood ratio test is

$$l_R = \frac{1}{N_0} \int_{T_i}^{T_f} \{2 \operatorname{Re}\,[\tilde{r}^*(t)\hat{\tilde{s}}_r(t)] - |\hat{\tilde{s}}_r(t)|^2\} \, dt \underset{H_0}{\overset{H_1}{\gtrless}} \gamma, \tag{149}$$

where $\hat{\tilde{s}}_r(t)$ is the realizable MMSE estimate of $\tilde{s}(t)$ when H_1 is true. An advantage of the implementation in (149) is that whenever $\tilde{s}(t)$ has a distributed state-variable representation we have a set of equations, (116)–(121), that specify $\hat{\tilde{s}}_r(t)$.

The approximate performance expressions that we derived earlier require knowledge of $\tilde{\mu}(s)$, which can be written in three different forms as

$$\tilde{\mu}(s) = \sum_{i=1}^{\infty} \left[(1 - s) \ln \left(1 + \frac{\tilde{\lambda}_i}{N_0} \right) - \ln \left(1 + (1 - s) \frac{\tilde{\lambda}_i}{N_0} \right) \right]. \quad (150)$$

or

$$\tilde{\mu}(s) = (1 - s) \ln \tilde{D}_{\mathscr{F}} \left(\frac{1}{N_0} \right) - \ln \tilde{D}_{\mathscr{F}} \left(\frac{1 - s}{N_0} \right), \quad (151)$$

or

$$\tilde{\mu}(s) = \frac{(1 - s)}{N_0} \int_{T_i}^{T_f} dt \left[\xi_P(t, \tilde{s}(t), N_0) - \xi_P \left(t, \tilde{s}(t), \frac{N_0}{1 - s} \right) \right]. \quad (152)$$

We evaluate one of these expressions to find the performance. Before discussing techniques for doing this, we formulate the communications model.

13.3.1.B.   Binary Communication. We consider a binary communication system using orthogonal signals. We transmit one of two orthogonal signals,

$$s_t(t) = \text{Re} \left[\sqrt{2E_t} \tilde{f}(t) e^{j\omega_1 t} \right], \qquad 0 \le t \le T : H_1, \quad (153)$$

$$s_t(t) = \text{Re} \left[\sqrt{2E_t} \tilde{f}(t) e^{j\omega_0 t} \right], \qquad 0 \le t \le T : H_0, \quad (154)$$

where $\tilde{f}(t)$ has unit energy. Notice that both transmitted signals have the same complex envelope but have different carrier frequencies. We discuss the choice of ω_0 and ω_1 in a moment. The two hypotheses are equally likely.

The received waveforms are

$$r(t) = \text{Re} \left[\sqrt{2} \, \tilde{s}_1(t) e^{j\omega_1 t} \right] + w(t), \qquad T_i \le t \le T_f : H_1, \quad (155)$$

$$r(t) = \text{Re} \left[\sqrt{2} \, \tilde{s}_0(t) e^{j\omega_0 t} \right] + w(t), \qquad T_i \le t \le T_f : H_0, \quad (156)$$

where

$$\tilde{s}_i(t) = \sqrt{E_t} \int_{-\infty}^{\infty} \tilde{f}(t - \lambda) \tilde{b}_i(t, \lambda) \, d\lambda, \qquad i = 0, 1. \quad (157)$$

The reflection processes $\tilde{b}_i(t, \lambda)$, $i = 0, 1$, are sample functions from zero-mean complex Gaussian processes, which can be characterized by the same scattering function, $\tilde{S}_{DR}\{f, \lambda\}$.

The channel has two effects on the transmitted signal. The first effect is a delay spread. If the scattering function has a length L, there would be a signal component in the received waveform over an interval of length $T + L$. The second effect is a frequency spread. If $\tilde{f}(t)$ is approximately bandlimited to a bandwidth of W cps and the scattering function is approximately bandlimited to B cps the signal portion of the received waveform is approximately bandlimited to $W + B$ cps.

We assume that $\omega_1 - \omega_0$ is large enough so that the signal components at the receiver are in disjoint frequency bands. We see that this separation must take into account both the transmitted signal bandwidth W and the channel-scattering function bandwidth B. Thus,

$$\frac{\omega_1 - \omega_0}{2\pi} > W + B. \tag{158}$$

The observation interval is $[T_i, T_f]$, and includes the entire interval in which there is a signal output. This implies

$$T_f - T_i \geq T + L. \tag{159}$$

The receiver must decide between two orthogonal bandpass Gaussian processes in the presence of additive white Gaussian noise. The criterion is minimum probability of error. This is a familiar problem (see Section 11.3). The optimum receiver consists of two parallel branches containing filters centered at ω_1 and ω_0. In the first branch we compute

$$l_1 \triangleq \int\int_{T_i}^{T_f} \tilde{r}^*(t)\tilde{h}(t, u)\tilde{r}(u)\, dt\, du, \tag{160}$$

where the complex representation is with respect to ω_1. In the other branch we compute

$$l_0 \triangleq \int\int_{T_i}^{T_f} \tilde{r}^*(t)\tilde{h}(t, u)\tilde{r}(u)\, dt\, du, \tag{161}$$

where the complex representation is with respect to ω_0. The complex impulse response is specified by

$$N_0\tilde{h}(t, u) + \int_{T_i}^{T_f} \tilde{h}(t, z)\tilde{K}_{\tilde{s}}(z, u)\, dz = \tilde{K}_{\tilde{s}}(t, u), \qquad T_i \leq t, u \leq T_f, \tag{162a}$$

where

$$\tilde{K}_{\tilde{s}}(t, u) = E_t \int_{-\infty}^{\infty} \tilde{f}(t - \lambda)\tilde{K}_{DR}(t - u, \lambda)\tilde{f}^*(u - \lambda)\, d\lambda. \tag{162b}$$

The optimum test is

$$l_1 \underset{H_0}{\overset{H_1}{\gtrless}} l_0, \tag{163}$$

as shown in Fig. 11.12. We see that (162a) is identical with (148). We can also write l_1 and l_0 in a form identical with (149). Thus, the equations specifying the optimum receiver are the same for the radar detection problem and the communication problem. Notice that the actual scattering functions will be different in the two problems, because of the different physical environments.

The performance calculation is appreciably simpler in the communication problem, because of the symmetric hypotheses and the zero threshold. Just as for the Doppler-spread case discussed in Section 11.3, we have tight bounds on the error probability. From (11.75),

$$\frac{e^{\tilde{\mu}_{\mathrm{BS}}(\frac{1}{2})}}{2[1 + \sqrt{(\pi/8)\ddot{\tilde{\mu}}_{\mathrm{BS}}(\frac{1}{2})}]} \le \Pr(\epsilon) \le \frac{e^{\tilde{\mu}_{\mathrm{BS}}(\frac{1}{2})}}{2[1 + \sqrt{\frac{1}{8}\ddot{\tilde{\mu}}_{\mathrm{BS}}(\frac{1}{2})}]} \le \frac{e^{\tilde{\mu}_{\mathrm{BS}}(\frac{1}{2})}}{2}, \tag{164}$$

where $\tilde{\mu}_{\mathrm{BS}}(s)$ can be expressed as

$$\tilde{\mu}_{\mathrm{BS}}(s) = \tilde{\mu}_{\mathrm{SIB}}(s) + \tilde{\mu}_{\mathrm{SIB}}(1 - s). \tag{165}$$

The subscript BS denotes binary symmetric, and the subscript SIB denotes simple binary. The formulas for $\tilde{\mu}_{\mathrm{SIB}}(s)$ were given in (150)–(152). Substituting (151) into (165) and simplifying gives

$$\tilde{\mu}_{\mathrm{BS}}(s) = \ln \left\{ \frac{\tilde{D}_{\mathscr{F}}(1/N_0)}{\tilde{D}_{\mathscr{F}}[(1 - s)/N_0]\tilde{D}_{\mathscr{F}}(s/N_0)} \right\}. \tag{166}$$

The exponent in (164) just involves

$$\begin{aligned}
\tilde{\mu}_{\mathrm{BS}}(\tfrac{1}{2}) &= \ln \left\{ \frac{\tilde{D}_{\mathscr{F}}(1/N_0)}{\tilde{D}_{\mathscr{F}}^2(1/2N_0)} \right\} \\
&= \sum_{i=1}^{\infty} \ln \left(1 + \frac{\tilde{\lambda}_i}{N_0} \right) - 2 \sum_{i=1}^{\infty} \ln \left(1 + \frac{\tilde{\lambda}_i}{2N_0} \right).
\end{aligned} \tag{167}$$

We can also write $\tilde{\mu}_{\mathrm{BS}}(\tfrac{1}{2})$ in terms of the realizable MMSE filtering error as

$$\tilde{\mu}_{\mathrm{BS}}(\tfrac{1}{2}) = \frac{1}{N_0} \int_{T_i}^{T_f} dt[\xi_P(t, \tilde{s}(t), N_0) - \xi_P(t, \tilde{s}(t), 2N_0)]. \tag{168}$$

The basic form of these expressions is familiar from Chapter 11. We must now develop a procedure for finding the required functions.

13.3.1.C.   Summary. In this section we have developed the model for the radar detection problem and the binary communication problem. The

equations specifying the optimum receivers and their performance were familiar. The new issue that we encountered is that of actually solving these equations when the covariance is given by (143).

There are two cases in which we can solve the equations in a reasonably straightforward manner. We identify them at this point and return to them later in the section. The first case is the low-energy-coherence (LEC) condition that we originally encountered in Chapter 4. We study this case in Section 13.3.4. The second case is a degenerate one in which we choose the transmitted signal so that the target or channel appears to be singly-spread. We discussed this degeneracy in Property 4 (22)–(29) on page 452 and shall study it again in Section 13.3.3. Although these two cases include many of the problems that we encounter in practice, we would like to be able to solve any doubly-spread target (or channel) problem. In the next two sections we develop techniques to deal with the general problem.

13.3.2 Approximate Models for Doubly-Spread Targets and Doubly-Spread Channels

In Section 13.3.1 we developed two methods of characterizing a doubly-spread target or channel:

1. The scattering function characterization.
2. The partial differential equation characterization.

These characterizations were easy to visualize and were taken as exact models of the actual physical phenomena. Unfortunately, except for a few special cases, we cannot solve the resulting equations specifying the optimum receiver and its performance.

In this subsection we develop some approximate channel models that allow us to compute the functions needed to specify the optimum receiver and its performance. Our discussion considers three models:

1. The tapped-delay line model.
2. The general orthogonal series model.
3. The approximate differential-equation model.

The tapped-delay line model is intuitively satisfying and relatively easy to implement, and so we present it first. The general orthogonal series model is a logical extension of the tapped-delay line model and leads to simpler computational requirements in many situations. The approximate differential-equation model leads to the general orthogonal series model in a different manner.

In all three cases, the complex envelope of the signal component is

$$\tilde{s}(t) = \sqrt{E_t} \int_{-\infty}^{\infty} \tilde{f}(t - \lambda)\tilde{b}(t, \lambda) \, d\lambda, \qquad -\infty < t < \infty, \qquad (169)$$

where we have assumed an infinite observation time for simplicity. The signal $\tilde{s}(t)$ is a sample function from a zero-mean Gaussian random process whose covariance function is given by (143).

The technique that we use in developing our approximate models is straightforward. We expand either $\tilde{f}(t - \lambda)$ or $\tilde{b}(t, \lambda)$ using a complete set of orthonormal functions. This enables us to replace the integral in (169) by an infinite sum. We then truncate the infinite series to obtain an approximate model. The various models differ in their choice of orthogonal functions.

It is important to remember that the "exact" model that we have been working with and the approximate models that we shall develop are both approximations to some physical target or channel. In most cases we have to estimate the target characteristics, and this introduces errors into our model. Thus, in many cases, the approximate models in the next section may represent the physical target or channel as effectively the exact model we have been using.

13.3.2.A.   Tapped-delay Line Model. We assume that the transmitted signal $\tilde{f}(t)$ is bandlimited around its carrier frequency. Thus,

$$\tilde{F}\{f\} = 0, \qquad |f| > \frac{W}{2}. \qquad (170)$$

Since $\tilde{f}(t)$ is bandlimited and the interval is infinite, a logical procedure is to expand $f(t - \lambda)$ using the sampling theorem. We write

$$\tilde{f}(t - \lambda) = \sum_{k=-\infty}^{\infty} \tilde{f}\left(t - \frac{k}{W_s}\right)\left(\frac{\sin \pi W_s(\lambda - k/W_s)}{\pi W_s(\lambda - k/W_s)}\right), \qquad (171)$$

where $W_s \geq W$. Notice that we could just let $W_s = W$ from the standpoint of the sampling theorem. Introducing W_s gives an additional flexibility in the model, which we shall exploit later.

Observe that we have put the λ dependence in the coordinate functions and the t dependence in the coefficients. This separation is the key to the series expansion approach. The $\sin x/x$ functions are orthogonal but not normalized. This is for convenience in interpreting the coefficients in (171) as samples. Substituting (171) into (169), we have

$$\tilde{s}(t) = \sqrt{E_t} \sum_{k=-\infty}^{\infty} \tilde{f}\left(t - \frac{k}{W_s}\right)\left[\int_{-\infty}^{\infty} \tilde{b}(t, \lambda) \frac{\sin \pi W_s(\lambda - k/W_s)}{\pi W_s(\lambda - k/W_s)}\right] d\lambda. \qquad (172)$$

If we define

$$\tilde{b}_k(t) \triangleq \int_{-\infty}^{\infty} \tilde{b}(t, \lambda) \frac{\sin \pi W_s(\lambda - k/W_s)}{\pi W_s(\lambda - k/W_s)} \, d\lambda, \tag{173}$$

then

$$\tilde{s}(t) = \sum_{k=-\infty}^{\infty} \tilde{f}\left(t - \frac{k}{W_s}\right) \tilde{b}_k(t). \tag{174}$$

Two observations regarding (174) are useful:

1. The functions $\tilde{f}(t - k/W_s)$ can be generated by passing $\tilde{f}(t)$ through a tapped-delay line with taps spaced $1/W_s$ seconds apart.

2. The functions $\tilde{b}_k(t)$, $-\infty < t < \infty$, are defined by (173). This weighted integration is sketched in Fig. 13.17. We see that if the scattering function has length L, $\tilde{b}_k(t)$ will be essentially zero for negative values of k and all positive values of k greater than LW_s.

These two observations lead us to the target (or channel) model shown in Fig. 13.18.†

The tap gains are sample functions from complex zero-mean Gaussian processes. To specify the model completely, we need their cross-covariance functions

$$E[\tilde{b}_k(t)\tilde{b}_l^*(u)]$$

$$= E\left\{\iint_{-\infty}^{\infty} \tilde{b}(t, \lambda)\tilde{b}^*(u, \lambda_1) \frac{\sin \pi W_s(\lambda - k/W_s)}{\pi W_s(\lambda - k/W_s)} \frac{\sin \pi W_s(\lambda_1 - l/W_s)}{\pi W_s(\lambda_1 - l/W_s)} \, d\lambda \, d\lambda_1\right\}. \tag{175}$$

Bringing the expectation inside the integral, using (37), and performing the integration with respect to λ_1, we have

$$E[\tilde{b}_k(t)\tilde{b}_l^*(u)]$$

$$= \int_{-\infty}^{\infty} \tilde{K}_{DR}(t - u, \lambda)\left[\frac{\sin \pi W_s(\lambda - k/W_s)}{\pi W_s(\lambda - k/W_s)}\right]\left[\frac{\sin \pi W_s(\lambda - l/W_s)}{\pi W_s(\lambda - l/W_s)}\right] d\lambda. \tag{176}$$

This expression is true for any $\tilde{K}_{DR}(t - u, \lambda)$.

The analysis is somewhat simpler if the tap gains are statistically independent. If $\tilde{K}_{DR}(t - u, \lambda)$ is essentially constant with respect to λ over $1/W_s$ units, the integral in (176) is *approximately* zero for $k \neq l$. If $\tilde{K}_{DR}(t - u, \lambda)$ is a smooth function of λ, we can improve the approximation by increasing W_s. Unfortunately, the dimension of the model increases as W_s increases. On page 500 we look at the effect of correlated
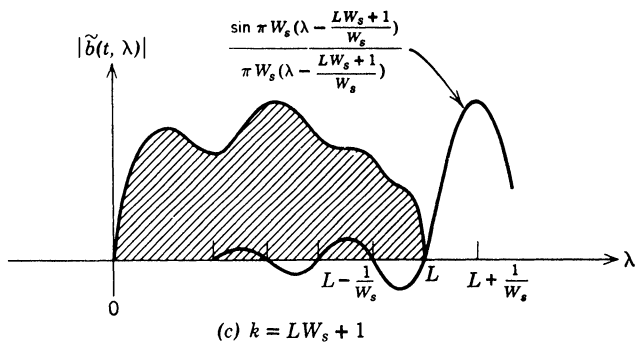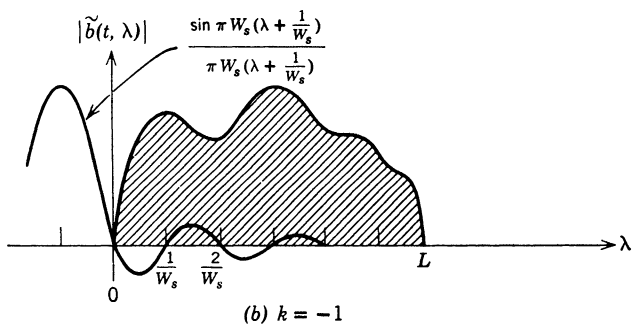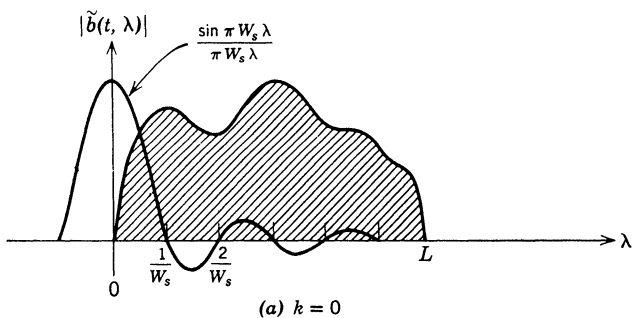
† The model in Fig. 13.18 is due to Kailath [35].

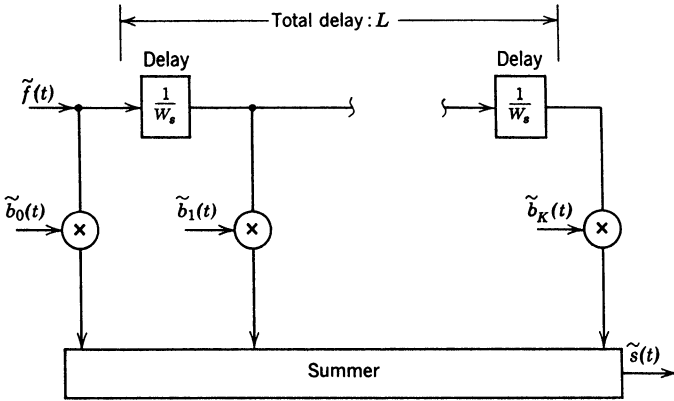Fig. 13.17 Location of sin x/x weighting function for various values of k.

Fig. 13.18 Tapped-delay line model for doubly-spread target (or channel).

coefficients. When the independent assumption is valid, we have

$$
E[\tilde{b}_k(t)\tilde{b}_l^*(u)] = \begin{cases} \dfrac{1}{W_s}\, \tilde{K}_{DR}\!\left(t - u, \dfrac{k}{W_s}\right), & k = l, \\[2mm] 0, & k \neq l. \end{cases} \tag{177}
$$

Because they are stationary, the tap gain processes can also be characterized in terms of their spectra. Transforming (177) gives

$$
\tilde{S}_{\tilde{b}_k}\{f\} = \frac{1}{W_s}\, \tilde{S}_{DR}\!\left(f, \frac{k}{W_s}\right). \tag{178}
$$

These spectra are just cross-sections of the scattering function at various values of λ.

We now have an approximate model for the target (or channel). Looking at (174), we see that we have replaced the doubly-spread channel by a set of $(K + 1)$ singly-spread channels whose signal output is

$$
\tilde{s}_K(t) = \sum_{k=0}^{K} \tilde{f}\!\left(t - \frac{k}{W_s}\right)\tilde{b}_k(t). \tag{179}
$$

This is a problem we can solve for a large class of channel processes.

As indicated by (149), the optimum receiver will contain $\hat{\tilde{s}}_{Kr}(t)$ as a waveform. Because $\tilde{f}(t)$ is known,

$$
\hat{\tilde{s}}_{Kr}(t) = \sum_{k=0}^{K} \tilde{f}\!\left(t - \frac{k}{W_s}\right)\hat{\tilde{b}}_{kr}(t). \tag{180}
$$

Thus the basic problem in implementing the optimum receiver is to generate the tap gain estimates and weight them with $\tilde{f}(t - k/W_s)$. The tapped-delay model has the advantage that the required functions can be generated

in a reasonably straightforward manner. We now discuss the design of the optimum receiver using the tapped-delay model.

If $\tilde{S}_{DR}\{f, \lambda\}$ is a rational function of f, each of the tap-gain functions has a finite state representation. When this is true, the optimum receiver and its performance can be evaluated using the techniques that we have already developed. To illustrate this, we set up the state-variable model.†

We assume that the scattering function is such that we need $(K + 1)$ taps. Then

$$\tilde{s}_K(t) = \sum_{k=0}^{K} \tilde{f}\left(t - \frac{k}{W_s}\right)\tilde{b}_k(t), \qquad T_i \le t \le T_f, \tag{181}$$

where $[T_i, T_f]$ is long enough so that essentially all the output signal energy is contained in the observation interval. The state vector for the kth tap gain is $\tilde{\mathbf{x}}_k(t)$, where

$$\dot{\tilde{\mathbf{x}}}_k(t) = \bar{\mathbf{F}}_k\tilde{\mathbf{x}}_k(t) + \bar{\mathbf{C}}_k\tilde{u}_k(t), \tag{182}$$

$$\tilde{b}_k(t) = \bar{\mathbf{C}}_k\tilde{\mathbf{x}}_k(t), \tag{183}$$

$$E[\tilde{u}_k(t)\tilde{u}_k^\dagger(\sigma)] = \tilde{Q}_k\,\delta(t - \sigma), \tag{184}$$

and

$$E[\tilde{\mathbf{x}}_k(T_i)\tilde{\mathbf{x}}_k^\dagger(T_i)] = \bar{\mathbf{P}}_k. \tag{185}$$

The dimension of the state vector is N_k.

The over-all state vector has the dimension

$$N = \sum_{k=0}^{K} N_k \tag{186}$$

and can be written as

$$\tilde{\mathbf{x}}(t) \triangleq \begin{bmatrix} \tilde{\mathbf{x}}_0(t) \\ \tilde{\mathbf{x}}_1(t) \\ \cdot \\ \cdot \\ \cdot \\ \tilde{\mathbf{x}}_K(t) \end{bmatrix}. \tag{187}$$

Then

$$\tilde{\mathbf{b}}(t) \triangleq \begin{bmatrix} \tilde{b}_0(t) \\ \tilde{b}_1(t) \\ \cdot \\ \cdot \\ \cdot \\ \tilde{b}_K(t) \end{bmatrix} = \begin{bmatrix} \bar{\mathbf{C}}_0 & & & \\ & \bar{\mathbf{C}}_1 & & 0 \\ & & \cdot & \\ & & & \cdot \\ 0 & & & \cdot \\ & & & & \bar{\mathbf{C}}_K \end{bmatrix}\tilde{\mathbf{x}}(t). \tag{188}$$

† This model is due to Van Trees [36].

The received signal process is just

$$\tilde{s}_K(t) = \left[\tilde{f}(t) \left| \tilde{f}\left(t - \frac{1}{W_s}\right) \right| \cdots \left| \tilde{f}\left(t - \frac{K}{W_s}\right) \right] \right] \tilde{b}(t) \triangleq \tilde{C}(t)\tilde{x}(t), \quad (189)$$

where $\tilde{C}(t)$ is defined by (188) and (189) as

$$\tilde{C}(t) \triangleq \left[\tilde{f}(t) \left| \tilde{f}\left(t - \frac{1}{W_s}\right) \right| \cdots \left| \tilde{f}\left(t - \frac{K}{W_s}\right) \right] \right] \begin{bmatrix} \tilde{C}_0 & & & \\ & \tilde{C}_1 & & 0 \\ & & \cdot & \\ & & & \cdot \\ 0 & & & \cdot \\ & & & & \tilde{C}_K \end{bmatrix}.$$

$$(190)$$

We have now reduced the problem to one that we have already solved [see (11.41–11.49)]. The complex receiver structure for the detection problem in (145) and (146) is shown in Fig. 13.19. (This is just the system in Fig. 11.9.) The optimum realizable filter is shown in Fig. 13.20. The only problem is the complexity of this system to generate $\hat{\tilde{s}}_{Kr}(t)$. This complexity is related to the dimension of the variance equation, which is an $N \times N$ matrix equation in this case. As usual, the variance equation can be solved before any data have been received.

To compute the performance, we evaluate $\tilde{\mu}(s)$ by using (152). Recall that $\tilde{\xi}_P(t, \tilde{s}(t), \cdot)$ is the realizable mean-square error in estimating $\tilde{s}(t)$ and is obtained from the solution to the variance equation.

It is important to emphasize that we have the problem in a form in which the optimum receiver and its performance can be calculated using straightforward numerical procedures. Notice that the dimension of the system grows quickly. An analytic solution is not feasible, but this is not important. We defer carrying out the details of an actual example until we complete our development of the various channel models.
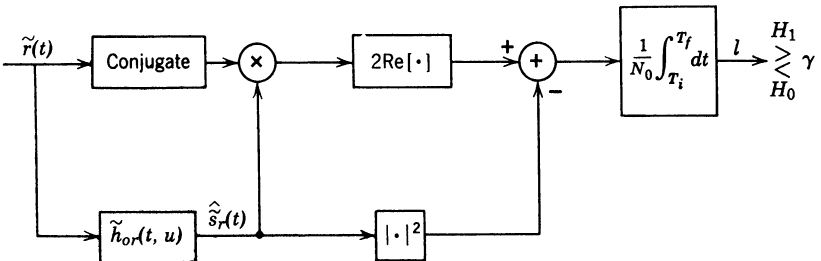

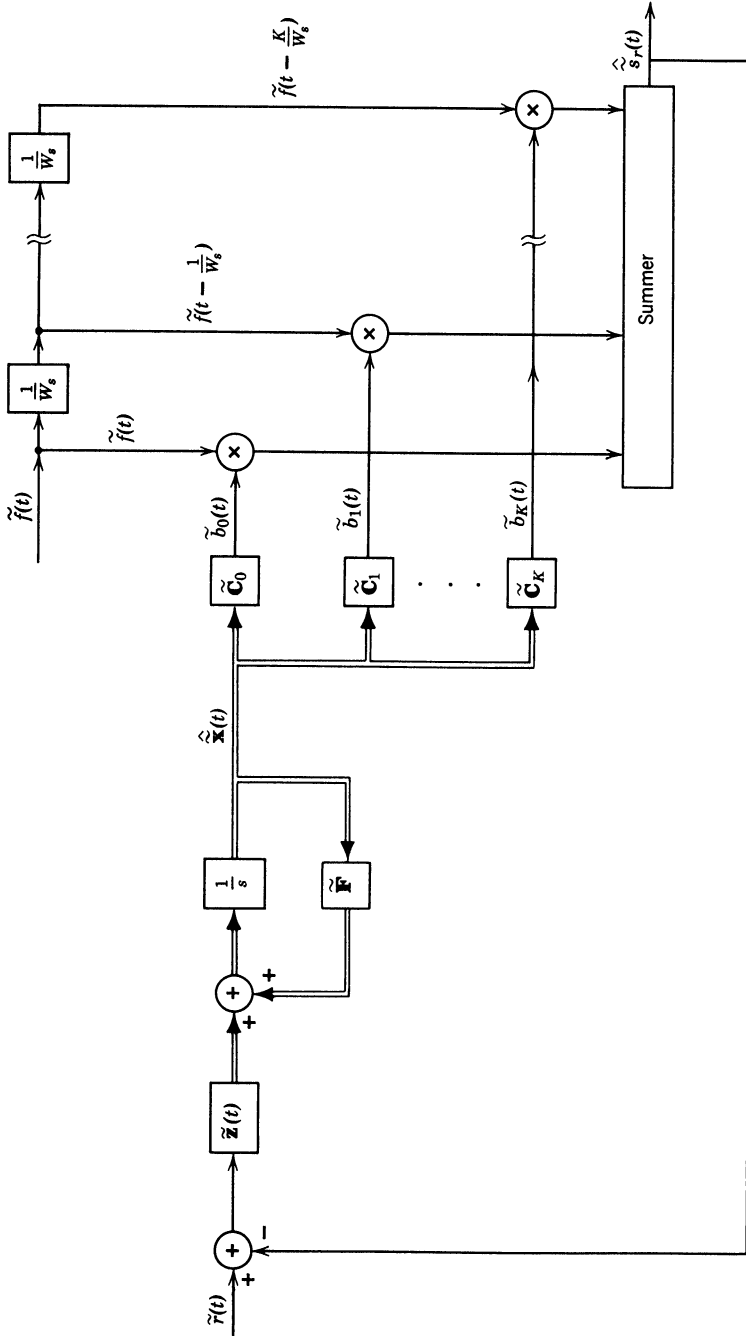Fig. 13.19 Optimum receiver for the detection of a doubly-spread target.

Fig. 13.20   Optimum realizable filter, $\tilde{h}_{or}(t, z)$, for tapped-delay line model.

13.3.2.B. General Orthogonal Series Model. The tapped-delay model has a great deal of intuitive appeal and is an adequate model for many physical situations. However, in many problems there are other orthogonal functions that provide a more efficient representation. In this section we develop a general model.

Our starting point is the differential-equation model of the channel that was introduced in Section 13.1.2. The state equation is

$$\frac{\partial \tilde{\mathbf{x}}(t, \lambda)}{\partial t} = \tilde{\mathbf{F}}(\lambda)\tilde{\mathbf{x}}(t, \lambda) + \tilde{\mathbf{G}}(\lambda)\tilde{u}(t, \lambda), \tag{191}$$

where

$$E[\tilde{u}(t, \lambda)\tilde{u}^*(t', \lambda')] = \tilde{Q}(\lambda)\delta(t - t')\,\delta(\lambda - \lambda'). \tag{192}$$

The initial condition of the state vector is

$$E[\tilde{\mathbf{x}}(T_0, \lambda)\tilde{\mathbf{x}}^\dagger(T_0, \lambda')] = \tilde{\mathbf{P}}_0(\lambda)\,\delta(\lambda - \lambda'). \tag{193}$$

The channel process is

$$\tilde{b}(t, \lambda) = \tilde{\mathbf{C}}(\lambda)\tilde{\mathbf{x}}(t, \lambda). \tag{194}$$

The signal component at the channel output is

$$\tilde{s}(t) = \sqrt{E_t}\int_{-\infty}^{\infty} \tilde{f}(t - \lambda)\tilde{b}(t, \lambda)\,d\lambda. \tag{195}$$

In the tapped-delay model we expanded the signal in an orthogonal series. In this case we represent the channel process and its state vector by a series expansion. We assume that the $\tilde{\varphi}_i(\lambda)$, $i = 1, 2, \ldots$, form a complete orthonormal set with

$$\int_{\Omega_L} \tilde{\varphi}_i(\lambda)\tilde{\varphi}_j^*(\lambda)\,d\lambda = \delta_{ij}, \tag{196}$$

where the interval Ω_L is the target (or channel) length. Notice that the $\tilde{\varphi}_i(\lambda)$ are an arbitrary set of orthonormal functions of λ only. We discuss methods of choosing the $\tilde{\varphi}_i(\lambda)$ later.

We first expand the state vector as

$$\tilde{\mathbf{x}}(t, \lambda) = \underset{K \to \infty}{\text{l.i.m.}}\ \tilde{\mathbf{x}}_K(t, \lambda) = \underset{K \to \infty}{\text{l.i.m.}} \sum_{i=1}^{K} \tilde{\mathbf{x}}_i(t)\tilde{\varphi}_i(\lambda), \qquad -\infty < t < \infty,\ \lambda \in \Omega_L, \tag{197}$$

where

$$\tilde{\mathbf{x}}_i(t) = \int_{\Omega_L} \tilde{\mathbf{x}}(t, \lambda)\tilde{\varphi}_i(\lambda)\,d\lambda, \qquad -\infty < t < \infty. \tag{198}$$

We expand the channel process, using the same set of orthonormal functions, as

$$\tilde{b}(t, \lambda) = \text{l.i.m.}_{K \to \infty} \tilde{b}_K(t, \lambda) = \text{l.i.m.}_{K \to \infty} \sum_{i=1}^{K} \tilde{b}_i(t)\tilde{\varphi}_i(\lambda), \qquad -\infty < t < \infty, \, \lambda \in \Omega_L,$$

(199)

where the $\tilde{b}_i(t)$ are determined by the requirement that

$$\tilde{b}_K(t, \lambda) = \tilde{C}(\lambda)\tilde{x}_K(t, \lambda), \qquad -\infty < t < \infty, \quad \lambda \in \Omega_L.$$

(200)

We refer to $\tilde{b}_K(t, \lambda)$ as the K-term approximation to the channel. We now develop a state-variable representation for $\tilde{b}_K(t, \lambda)$.

From (197),

$$\frac{\partial \tilde{x}(t, \lambda)}{\partial t} = \sum_{j=1}^{\infty} \frac{d\tilde{x}_j(t)}{dt} \tilde{\phi}_j(\lambda).$$

(201)

Substituting (197) and (201) into (191) gives

$$\sum_{j=1}^{\infty} \frac{d\tilde{x}_j(t)}{dt} \tilde{\phi}_j(\lambda) = \tilde{F}(\lambda)\sum_{j=1}^{\infty} \tilde{x}_j(t)\tilde{\phi}_j(\lambda) + \tilde{G}(\lambda)\tilde{u}(t, \lambda).$$

(202)

Multiplying both sides of (202) by $\tilde{\phi}_i^*(\lambda)$ and integrating with respect to λ over Ω_L, we obtain

$$\frac{d\tilde{x}_i(t)}{dt} = \sum_{j=1}^{\infty} \left[\int_{\Omega_L} \tilde{F}(\lambda)\tilde{\phi}_i^*(\lambda)\tilde{\phi}_j(\lambda) \, d\lambda \right] \tilde{x}_j(t) + \int_{\Omega_L} \tilde{G}(\lambda)\tilde{u}(t, \lambda)\tilde{\phi}_i^*(\lambda) \, d\lambda.$$

(203)

We now define

$$\tilde{F}_{ij} \triangleq \int_{\Omega_L} \tilde{F}(\lambda)\tilde{\phi}_i^*(\lambda)\tilde{\phi}_j(\lambda) \, d\lambda, \qquad i, j = 1, 2, \dots$$

(204)

and

$$\tilde{u}_i(t) = \int_{\Omega_L} G(\lambda)\tilde{u}(t, \lambda)\tilde{\phi}_i^*(\lambda) \, d\lambda, \qquad i = 1, 2, \dots.$$

(205)

Truncating the series gives a K-term approximation to the channel state vector. The state equation is

$$\frac{d}{dt}
\begin{bmatrix}
\tilde{x}_1(t) \\
\tilde{x}_2(t) \\
\cdot \\
\cdot \\
\cdot \\
\tilde{x}_K(t)
\end{bmatrix}
=
\begin{bmatrix}
\tilde{F}_{11} & \tilde{F}_{12} & \tilde{F}_{13} & & \tilde{F}_{1K} \\
\tilde{F}_{21} & \tilde{F}_{22} & & & \\
\tilde{F}_{31} & & & & \\
& & & & \\
\tilde{F}_{K1} & & & & \tilde{F}_{KK}
\end{bmatrix}
\begin{bmatrix}
\tilde{x}_1(t) \\
\tilde{x}_2(t) \\
\cdot \\
\cdot \\
\cdot \\
\tilde{x}_K(t)
\end{bmatrix}
+
\begin{bmatrix}
\tilde{u}_1(t) \\
\tilde{u}_2(t) \\
\cdot \\
\cdot \\
\cdot \\
\tilde{u}_K(t)
\end{bmatrix}.$$

(206)

If the original distributed state vector is N-dimensional, the state vector in (206) has NK dimensions. We can write (206) compactly as

$$\frac{d\tilde{\mathbf{x}}_{\mathbf{M}}(t)}{dt} = \bar{\mathbf{F}}_{\mathbf{M}}(\lambda)\tilde{\mathbf{x}}_{\mathbf{M}}(t) + \bar{\mathbf{u}}_{\mathbf{M}}(t). \tag{207}$$

The subscript **M** denotes model. The elements in the covariance function matrix of the driving function are

$$E[\mathbf{u}_i(t)\mathbf{u}_j^\dagger(t')] = E\left\{ \int_{\Omega_L} \tilde{\mathbf{G}}(\lambda)\tilde{u}(t,\lambda)\tilde{\phi}_i^*(\lambda)\,d\lambda \int_{\Omega_L} \tilde{\mathbf{G}}^\dagger(\lambda')\tilde{u}^*(t',\lambda')\tilde{\phi}_j(\lambda')\,d\lambda' \right\}$$

$$= \left[\int_{\Omega_L} \tilde{\mathbf{G}}(\lambda)\tilde{\mathbf{Q}}(\lambda)\tilde{\mathbf{G}}^\dagger(\lambda)\tilde{\phi}_i^*(\lambda)\tilde{\phi}_j(\lambda)\,d\lambda \right]\delta(t-t')$$

$$\triangleq \tilde{\mathbf{Q}}_{ij}\delta(t-t'). \tag{208}$$

The initial conditions are

$$E[\tilde{\mathbf{x}}_i(T_0)\tilde{\mathbf{x}}_j^\dagger(T_0)] = E\left[\int_{\Omega_L} \tilde{\mathbf{x}}(T_0,\lambda)\tilde{\phi}_i^*(\lambda)\,d\lambda \int_{\Omega_L} \tilde{\mathbf{x}}^\dagger(T_0,\lambda')\tilde{\phi}_j(\lambda')\,d\lambda' \right]$$

$$= \int_{\Omega_L} \tilde{\mathbf{K}}_{\tilde{x}}(\lambda)\tilde{\phi}_i^*(\lambda)\tilde{\phi}_j(\lambda)\,d\lambda, \tag{209}$$

where $\tilde{\mathbf{K}}_{\tilde{x}}(\lambda)$ is defined in (46).

We must now find the observation matrix relating $\tilde{b}_i(t)$ to $\tilde{\mathbf{x}}_{\mathbf{M}}(t)$. Using (197), (199), and (200), we have

$$\sum_{j=1}^{K} \tilde{b}_j(t)\tilde{\varphi}_j(\lambda) = \tilde{\mathbf{C}}(\lambda)\sum_{j=1}^{K} \tilde{\mathbf{x}}_j(t)\tilde{\varphi}_j(\lambda). \tag{210}$$

Multiplying both sides by $\tilde{\varphi}_i^*(\lambda)$ and integrating over Ω_L gives

$$\tilde{b}_i(t) = \sum_{j=1}^{K} \left[\int_{\Omega_L} \tilde{\varphi}_i^*(\lambda)\tilde{\mathbf{C}}(\lambda)\tilde{\varphi}_j(\lambda)\,d\lambda \right]\tilde{\mathbf{x}}_j(t). \tag{211}$$

Defining

$$\tilde{\mathbf{C}}_{ij} = \int_{\Omega_L} \tilde{\varphi}_i^*(\lambda)\tilde{\mathbf{C}}(\lambda)\tilde{\varphi}_j(\lambda)\,d\lambda, \tag{212}$$

we obtain

$$\tilde{b}_i(t) = [\tilde{\mathbf{C}}_{i1} \vdots \tilde{\mathbf{C}}_{i2} \vdots \cdots \tilde{\mathbf{C}}_{iK}]\tilde{\mathbf{x}}_{\mathbf{M}}(t)$$

$$\triangleq \tilde{\mathbf{C}}_{i\mathbf{M}}\tilde{\mathbf{x}}_{\mathbf{M}}(t). \tag{213}$$

The signal component at the output of the channel is

$$\tilde{s}(t) = \sqrt{E_t}\int_{-\infty}^{\infty} \tilde{f}(t-\lambda)\tilde{b}(t,\lambda)\,d\lambda. \tag{214}$$

The K-term approximation is

$$\tilde{s}_K(t) = \sqrt{E_t} \int_{-\infty}^{\infty} \tilde{f}(t - \lambda) \sum_{i=1}^{K} \tilde{b}_i(t)\tilde{\varphi}_i(\lambda) \, d\lambda$$

$$= \sum_{i=1}^{K} \tilde{f}_i \tilde{b}_i(t), \tag{215}$$

where

$$\tilde{f}_i \triangleq \sqrt{E_t} \int_{-\infty}^{\infty} \tilde{f}(t - \lambda)\tilde{\varphi}_i(\lambda) \, d\lambda. \tag{216}$$

Using (213) in (215), we obtain

$$\tilde{s}_K(t) = \left(\sum_{i=1}^{K} \tilde{f}_i \bar{\mathbf{C}}_{i\mathbf{M}}\right) \tilde{\mathbf{x}}_{\mathbf{M}}(t)$$

$$\triangleq \bar{\mathbf{C}}_{\mathbf{M}} \tilde{\mathbf{x}}_{\mathbf{M}}(t). \tag{217}$$

We now have the K-term approximation to the problem completely characterized by a state-variable representation. Once we have this representation, all the results in Section 11.2.2 are immediately applicable. Notice that, although the formulas appear complicated, all the necessary quantities can be calculated in a straightforward manner.

Two comments regarding the model are worthwhile.

1. The tapped-delay line model is a special case of this model (see Problem 13.3.9).

2. The proper choice of the orthogonal set will depend on the scattering function and the signal. A judicious choice will simplify both the structure of the state equation and the value of K required to get a good approximation. It is this simplification in the state equation that has motivated the development of the general orthogonal series model. In the next section we illustrate the choice of the orthogonal set for a typical example.

Up to this point in this section, we have considered various orthogonal series models for doubly-spread channels. The goal was to obtain a finite-dimensional approximation that we could analyze completely. We now consider a direct analysis of the differential-equation model.

13.3.2.C.   Approximate Differential-equation Model.† The differential-equation model for the doubly-spread channel was described by (38)–(41), which are repeated here for convenience. The state equation is

$$\frac{\partial \tilde{\mathbf{x}}(t, \lambda)}{\partial t} = \bar{\mathbf{F}}(\lambda)\tilde{\mathbf{x}}(t, \lambda) + \tilde{\mathbf{G}}(\lambda)\tilde{u}(t, \lambda), \tag{218}$$

† The results in this section are due to Kurth [7].

where

$$E[\tilde{u}(t, \lambda)\tilde{u}^*(t', \lambda')] = \tilde{Q}(\lambda)\,\delta(t - t')\,\delta(\lambda - \lambda'). \tag{219}$$

The initial covariance of the state vector is

$$E[\tilde{\mathbf{x}}(T_i, \lambda)\tilde{\mathbf{x}}^\dagger(T_i, \lambda')] = \tilde{\mathbf{P}}_0(\lambda)\,\delta(\lambda - \lambda'). \tag{220}$$

The channel process is

$$\tilde{b}(t, \lambda) = \tilde{\mathbf{C}}(\lambda)\tilde{\mathbf{x}}(t, \lambda). \tag{221}$$

The signal component at the channel output is

$$\tilde{s}(t) = \int_{-\infty}^{\infty} \tilde{f}(t - \lambda)\tilde{b}(t, \lambda)\,d\lambda. \tag{222}$$

The optimum test can be written in terms of the MMSE realizable estimate of $\tilde{s}(t)$. From (149),

$$\boxed{l_R = \frac{1}{N_0}\int_{T_i}^{T'}\{2\,\mathrm{Re}\,[\tilde{r}^*(t)\hat{\tilde{s}}_r(t)] - |\hat{\tilde{s}}_r(t)|^2\}\,dt.} \tag{223}$$

Notice that $\tilde{s}(t)$ is a function of time only, so that the derivation leading to (149) is applicable without any modification.

To implement the test, we need an expression for $\hat{\tilde{s}}_r(t)$. These equations were encountered previously in Section 13.2.2 (116)–(121). The estimator equation is

$$\frac{\partial \hat{\tilde{\mathbf{x}}}(t, \lambda)}{\partial t} = \tilde{\mathbf{F}}(\lambda)\tilde{\mathbf{x}}(t, \lambda) + \tilde{\mathbf{z}}(t, \lambda)[\tilde{r}(t) - \tilde{s}(t:\hat{\tilde{\mathbf{x}}}(t, \lambda))], \qquad t \geq T_i, \lambda \in \Omega_L, \tag{224}$$

and

$$\hat{\tilde{\mathbf{x}}}(T_i, \lambda) = \mathbf{0}, \qquad \lambda \in \Omega_L. \tag{225}$$

The gain equation is

$$\tilde{\mathbf{z}}(t, \lambda) = \frac{1}{N_0}\left[\int_{\Omega_L}\tilde{\boldsymbol{\xi}}(t:\lambda, \lambda')\tilde{\mathbf{C}}^\dagger(\lambda')\sqrt{E_t}\tilde{f}^*(t - \lambda')\,d\lambda'\right]. \tag{226}$$

The variance equation is

$$\frac{\partial \tilde{\boldsymbol{\xi}}(t:\lambda, \lambda')}{\partial t} = \tilde{\mathbf{F}}(\lambda)\tilde{\boldsymbol{\xi}}(t:\lambda, \lambda') + \tilde{\boldsymbol{\xi}}^\dagger(t:\lambda', \lambda)\tilde{\mathbf{F}}^\dagger(\lambda') + \tilde{\mathbf{G}}(\lambda)\tilde{Q}(\lambda)\tilde{\mathbf{G}}^\dagger(\lambda')$$

$$- \frac{1}{N_0}\left\{\int_{\Omega_L}\tilde{\boldsymbol{\xi}}(t:\lambda, \sigma)\tilde{\mathbf{C}}^\dagger(\sigma)\sqrt{E_t}\tilde{f}^*(t - \sigma)\,d\sigma\right.$$

$$\left.\times \int_{\Omega_L}\sqrt{E}\tilde{f}(t - \sigma')\tilde{\mathbf{C}}(\sigma')\tilde{\boldsymbol{\xi}}(t:\sigma', \lambda')\,d\sigma'\right\},$$

$$\lambda, \lambda' \in \Omega_L, t \geq T_i, \tag{227}$$

with the initial condition

$$\breve{\boldsymbol{\xi}}(T_i : \lambda, \lambda') = \breve{\boldsymbol{\xi}}_0(T_i, \lambda)\, \delta(\lambda - \lambda'),$$
$$= \tilde{\mathbf{K}}_{\tilde{x}}(\lambda)\, \delta(\lambda - \lambda'). \tag{228}$$

The expressions in (224)–(228) characterize the channel estimator. Using these equations, (222) and (223) give the optimum receiver that was shown in Fig. 13.19. We are still faced with the problem of implementing (224)–(228) in order to generate $\hat{\tilde{s}}_r(t)$. A block diagram of a system containing spatial operations that could be used to generate $\hat{\tilde{s}}_r(t)$ was shown in Fig. 13.15 [replace $\hat{\tilde{n}}_r(t)$ with $\hat{\tilde{s}}_r(t)$]. In general we cannot implement this system and must be content with an approximate solution. We consider three procedures for obtaining an approximate solution.

The first procedure is to expand the state vector in an orthonormal expansion and truncate the expansion at K terms. This procedure takes us back to the model on pages 495–498. A second procedure is to sample in λ. The resulting model would be similar to the tapped-delay line model derived in Section 13.3.2.A, but the tap gains would be correlated. This procedure is generally inefficient from the computational standpoint.

We now develop a third procedure that seems to offer some computational advantages. The first step is to divide the covariance matrix into an impulsive term and bounded term as

$$\breve{\boldsymbol{\xi}}(t : \lambda, \lambda') = \breve{\boldsymbol{\xi}}_0(T_i, \lambda)\, \delta(\lambda - \lambda') + \tilde{\mathbf{p}}(t : \lambda, \lambda'), \qquad \lambda, \lambda' \in \Omega_L, t \geq T_i. \tag{229}$$

Substituting (229) into (227), we find that $\tilde{\mathbf{p}}(t : \lambda, \lambda')$ must satisfy the differential equation

$$\frac{\partial \tilde{\mathbf{p}}(t : \lambda, \lambda')}{\partial t} = \tilde{F}(\lambda)\tilde{\mathbf{p}}(t : \lambda, \lambda') + \tilde{\mathbf{p}}(t : \lambda, \lambda')\tilde{\mathbf{F}}^\dagger(\lambda')$$

$$- \frac{1}{N_0}\Bigg\{\Bigg[\, \tilde{\mathbf{K}}_{\tilde{x}}(\lambda)\tilde{\mathbf{C}}^\dagger(\lambda)\sqrt{E_t}\tilde{f}(t - \lambda)$$

$$+ \int_{\Omega_L} \tilde{\mathbf{p}}(t : \lambda, \sigma)\tilde{\mathbf{C}}^\dagger(\sigma)\sqrt{E_t}\tilde{f}^*(t - \sigma)\, d\sigma \Bigg]$$

$$\times \Bigg[\sqrt{E_t}\tilde{f}(t - \lambda')\tilde{\mathbf{C}}(\lambda')\mathbf{K}_{\tilde{x}}(\lambda')$$

$$+ \int_{\Omega_L} \sqrt{E_t}\tilde{f}(t - \sigma')\tilde{\mathbf{C}}(\sigma')\tilde{\mathbf{p}}(t : \sigma', \lambda')\, d\sigma' \Bigg]\Bigg\},$$

$$t \geq T_i, \lambda, \lambda' \in \Omega_L, \tag{230}$$

with the zero initial condition

$$\tilde{\mathbf{p}}(t:\lambda, \lambda') = \mathbf{0}. \tag{231}$$

We then expand $\tilde{\mathbf{p}}(t:\lambda, \lambda')$ in a series expansion as

$$\tilde{\mathbf{p}}(t:\lambda, \lambda') = \sum_{i=1}^{\infty} \sum_{j=1}^{\infty} \tilde{\mathbf{p}}_{ij}(t)\tilde{\phi}_i(\lambda)\tilde{\phi}_j^*(\lambda'), \qquad \lambda, \lambda' \in \Omega_L, \qquad t \geq T_i, \tag{232}$$

where the $\tilde{\phi}_i(\lambda)$ are an arbitrary set of orthonormal functions and

$$\tilde{\mathbf{p}}_{ij}(t) \triangleq \int_{\Omega_L} d\lambda \int_{\Omega_L} d\lambda' \tilde{\mathbf{p}}(t:\lambda, \lambda')\tilde{\phi}_i(\lambda)\tilde{\phi}_j^*(\lambda'). \tag{233}$$

This procedure is referred to as a *modal expansion technique.*

We truncate the series at $i = j = K$ to obtain an approximate solution. Proceeding as before, we can derive a set of differential equations specifying the $\tilde{\mathbf{p}}_{ij}(t)$ (see Problem 13.3.12). The advantage of separating out the impulse in (229) is that the convergence of the series approximation is usually better. We shall apply this third procedure to a specific problem in Section 13.3.3.

The final step is to compute the performance. We do this by evaluating $\tilde{\mu}(s)$ and using it in our approximate error expressions. We can express $\tilde{\mu}(s)$ in terms of the realizable MMSE signal estimation error, $\xi_P(t, \tilde{s}(t), \cdot)$, by (11.54). Finally, we express $\xi_P(t, \tilde{s}(t), N_0)$ in terms of $\xi_P(t:\lambda, \lambda')$.

$$\xi_P(t, \tilde{s}(t), N_0) \triangleq E[|\tilde{s}(t) - \hat{s}(t)|^2]. \tag{234}$$

Using (221) and (222) in (234) gives

$$\xi_P(t, \tilde{s}(t), N_0) = \int_{\Omega_L} d\sigma \int_{\Omega_L} d\sigma' E_t \tilde{f}(t - \sigma)\tilde{\mathbf{C}}(\sigma)\tilde{\boldsymbol{\xi}}(t:\sigma, \sigma')\tilde{\mathbf{C}}^{\dagger}(\sigma')\tilde{f}^*(t - \sigma'). \tag{235}$$

Notice that to find $\tilde{\mu}(\frac{1}{2})$ we must solve the variance equation (227) for two values of the additive noise level, N_0 and $2N_0$. To find $\tilde{\mu}(s)$, in general, we must solve the variance equation for three values of the additive noise level.

13.3.2.D. Summary of Approximate Model Discussion.

In this subsection we have developed various models that we can use to approximate a doubly-spread target (or channel). The advantage of all these models is that they enable us to obtain a complete solution for the optimum receiver and its performance.

As we pointed out in the introduction to Section 13.3.3, the tapped-delay line model is the simplest to implement and is the only model that has been used in actual systems. At their present state of development,

the other two models are most useful in the study of performance limitations.

There are many approximate channel models in addition to those that we have discussed. Suitable references are [35], [61], and [64].

13.3.3   Binary Communication over Doubly-Spread Channels

In Section 13.3.1.B we formulated a model for a binary FSK system operating over a doubly-spread channel [see (153)–(168)]. In this section we continue our discussion of the communication problem.

Our discussion is divided into three parts. In Section 13.3.3.A we discuss the performance bounds on binary communication systems and demonstrate some simple signaling schemes that approach these bounds. In Section 13.3.3.B we carry out a detailed performance analysis of a specific system using one of the approximate channel models developed in Section 13.3.2. In Section 13.3.3.C we discuss suboptimum receivers briefly.

13.3.3.A.   Performance Bounds and Efficient Systems. As we pointed out in Section 13.3.1.B, the decision problem is that of detecting a complex Gaussian process in complex white Gaussian noise. The covariance function of the signal process, $\tilde{s}(t)$, is given by (5) as

$$\tilde{K}_{\tilde{s}}(t, u) = E_t \int_{-\infty}^{\infty} \tilde{f}(t - \lambda) \tilde{K}_{DR}(t - u, \lambda) \tilde{f}^*(u - \lambda) \, d\lambda. \qquad (236)$$

The performance will depend on E_t, N_0, $\tilde{f}(t)$, and $\tilde{K}_{DR}(t - u, \lambda)$ and may be difficult to evaluate in the general case. However, in Section 11.3 we derived a bound on how well any binary system could perform for a given E_t and N_0. Since this bound only depended on the eigenvalues of $\tilde{s}(t)$, it is still valid in this problem.

On page 380 we demonstrated that in order to achieve the bound we would like to design the signal so that the output process has D_o equal eigenvalues, where

$$D_o = \frac{\bar{E}_r / N_0}{3.07} \qquad (237)$$

and

$$\bar{E}_r = E_t \iint\limits_{-\infty}^{\infty} \tilde{S}_{DR}\{f, \lambda\} \, df \, d\lambda. \qquad (238)$$

For this optimum case,

$$\tilde{\mu}_{\mathrm{BS}}(\tfrac{1}{2}) = -0.1488 \left(\frac{\bar{E}_r}{N_0} \right). \qquad (239)$$

Thus, the probability of error using any signal $\tilde{f}(t)$ is bounded by

$$\Pr(\epsilon) \le \tfrac{1}{2} \exp\left(-0.1488 \frac{\bar{E}_r}{N_0}\right). \tag{240}$$

This gives us a simple bound on the probability of error for binary orthogonal signals. The difficulty is that there is no guarantee that a signal exists that enables us to achieve this performance. We now discuss two situations in which we can approach the bound with simple signals.

UNDERSPREAD CHANNELS. In (32) we defined an underspread channel as one whose BL product was less than 1. We now discuss the problem of communicating over an underspread channel. (Notice that we allow $B \gg 1$ or $L \gg 1$, as long as $BL \ll 1$.)

In our discussion of communication over Doppler-spread channels in Section 11.3 (specifically pages 384–385), we saw that we could achieve the bound in (240) for any scattering function if there were no peak-power or time-duration constraints. The required signal consisted of a sequence of short pulses, with the number of pulses chosen to achieve the optimum diversity specified in (237) [i.e., $n = D_o$]. The length T of each pulse was much less than B^{-1} (the reciprocal of the bandwidth of the Doppler spread), so that there was no time-selective fading. Here we achieved the desired eigenvalue distribution by reducing the channel to a set of non-fluctuating point channels.

We now consider a similar system for signaling over a doubly-spread channel. The signal is shown in Fig. 13.21. To avoid time-selective fading, we require that

$$T \ll \frac{1}{B}. \tag{241}\dagger$$

To avoid frequency-selective fading, we require that

$$W \ll \frac{1}{L}. \tag{242}$$

Combining (241) and (242), we see that the requirement for flat (nonselective) fading is

$$WT \lll \frac{1}{BL}. \tag{243}$$

However, we know that for any signal

$$WT \ge 1. \tag{244}$$

---

† Our discussion uses B and W as imprecise bandwidth measures. An exact definition is not needed in the current context.
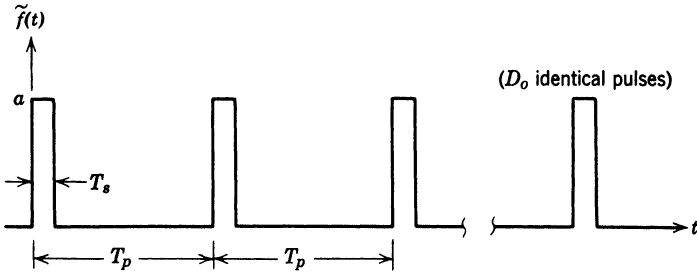
Fig. 13.21 Signal for communication over an underspread channel.

Therefore we require that

$$BL \lll 1 \qquad (245)$$

in order for us to be able to satisfy (243). The condition in (245) can only be met by underspread channels [see (32)]. The condition in (245) is stronger than the underspread requirement of (32). If the condition in (245) is satisfied and there is no peak-power or time-duration constraint, we can achieve the bound in (240) by using the signal in Fig. 13.21 with its parameters chosen optimally.

We should observe that the requirement in (245) is usually too strict. In many cases we can come close to the performance in (240) with the signal in Fig. 13.21 for BL products approaching unity.

We next consider the case in which BL exceeds unity.

OVERSPREAD CHANNELS. If $BL > 1$, we cannot have fading that is flat in both time and frequency. However, we can choose the signal so that we have either time-selective fading or frequency-selective fading, but not both. We demonstrate this with a simple example.

Example. We consider an idealized channel whose scattering function is shown in Fig 13.22. We assume that

$$BL = 5. \qquad (246)$$

We transmit a long rectangular pulse

$$\tilde{f}(t) = \begin{cases} \sqrt{\dfrac{1}{T}}, & 0 < t < T, \\ \\ 0, & \text{elsewhere,} \end{cases} \qquad (247)$$

We also require that

$$T \geq 10L. \qquad (248)$$

Comparing (248) and (242), we see that we can treat the channel as a Doppler-spread channel. From the results in Example 1 of Chapter 11, we know that if

$$2BT = \frac{\bar{E}_r/N_0}{3.07}, \qquad (249)$$
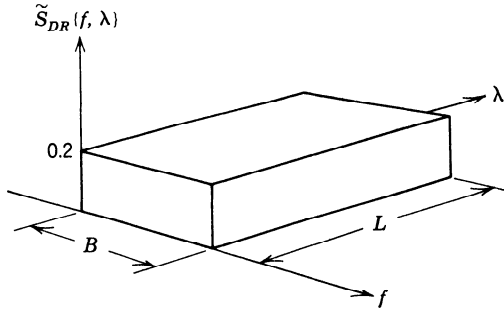
$\tilde{S}_{DR}(f, \lambda)$

Fig. 13.22 An idealized scattering function.

we shall achieve the bound in (240). Using (246) and (248) in (249), we obtain the requirement

$$\frac{\bar{E}_r}{N_0} \geq 307, \tag{250}$$

which is unrealistic [the $\Pr(\epsilon) \simeq 10^{-21}$].

We can obtain a more realistic solution by relaxing some of the requirements. For example, if we require that

$$T \geq \tfrac{10}{3}L \tag{251}$$

and

$$2BT = \frac{1}{2}\frac{\bar{E}_r/N_0}{3.07}, \tag{252}$$

then

$$\frac{\bar{E}_r}{N_0} \geq 60 \tag{253}$$

is adequate. The system in (251)–(253) is realistic and will perform close to the bound.

This example illustrates one procedure for signaling efficiently over an overspread channel. The basic principle involved is straightforward. The doubly-spread channel provides a certain amount of implicit diversity in the output signal. If the value of $\bar{E}_r/N_0$ is large enough to make this amount of diversity close to optimum, the system will work close to the bound. On the other hand, if $\bar{E}_r/N_0$ is too small, the performance may be relatively poor.

SUMMARY. In this section we have discussed the performance bounds that apply to any binary system. In addition, we have studied possible signaling schemes for underspread and overspread channels. In the underspread case we could use a signal that reduced the channel to a set of nonfluctuating point channels. By selecting the correct number of subpulses, we could achieve the bound. In the overspread case we could use a signal that reduced the channel to a singly-spread channel. In this case we could approach the bound if the available $\bar{E}_r/N_0$ was large enough.

In both cases we were able to use signals that eliminated the double spreading in the channel. This has several advantages:

1. The optimum receiver is simpler.
2. The performance analysis is simpler.
3. The performance is close enough to the bound that using the channel in a doubly-spread mode could not provide a significant decrease in the error probability.

It appears that in a large number of physical situations we can achieve this simplification, so that the above discussion is relevant. On the other hand, there are at least two reasons why we want to be able to analyze the doubly-spread model directly:

1. There are cases in which we cannot simplify the channel, because of limitations on the signal duration or bandwidth.
2. There is a transitional region between the singly- and doubly-spread cases in which we must check our intuitive arguments; in this region the gross signal and channel characterizations (W, T, B, and L) are not adequate.

In Section 13.3.2 we developed the necessary models to carry out this analysis. In the next section we use these models to analyze the binary communication problem.

13.3.3.B.   Performance Analysis for a Specific System.† In Section 13.3.2 we developed approximate channel models with which we could design the optimum receiver and analyze its performance. We now consider a specific system to illustrate the details of the technique. The discussion has two distinct purposes. The first purpose is to demonstrate with an example the actual steps that one must go through to analyze the system performance. This detailed discussion illustrates the ideas of Section 13.3.2 and enables the reader to analyze any system of interest. The second purpose is to provide an understanding of the important issues in a communication system operating over a doubly-spread channel. The relationship between the signal parameters and the scattering function is explored. The quantitative results apply only to this specific system, but the approach can be used in other problems. This discussion will augment the results in Section 13.3.3.A.

The binary communication problem is described in (153)–(168). The channel-scattering process is described by (38)–(51). We consider a scattering function that is a special case of the scattering function in the example on

---

† The material in Subsection 13.3.3.B is due to Kurth [7].

page 456. The functions specifying it are

$$\tilde{Q}(\lambda) = \frac{2k}{L}\left[1 - \cos\left(\frac{2\pi\lambda}{L}\right)\right]\amalg_L(\lambda), \tag{254}$$

where $\amalg_L(\lambda)$ is a gate function defined as

$$\amalg_L(\lambda) = \begin{cases} 1, & 0 \le \lambda \le L, \\ 0, & \text{elsewhere.} \end{cases} \tag{255}$$

In addition,

$$\tilde{k}(\lambda) = k \tag{256}$$

and

$$\tilde{C}(\lambda) = 1. \tag{257}$$

Notice that in this simple problem

$$\tilde{b}(t, \lambda) = \tilde{x}(t, \lambda). \tag{258}$$

The scattering function is

$$\tilde{S}_{DR}\{f, \lambda\} = \frac{\tilde{Q}(\lambda)}{(2\pi f)^2 + k^2}. \tag{259}$$

To use (230), we need $\tilde{K}_{\tilde{x}}(\lambda)$. Recalling from (46)–(49) that

$$\tilde{K}_{\tilde{x}}(\lambda) = \tilde{K}_{DR}(0, \lambda), \tag{260}$$

we have

$$\tilde{K}_{\tilde{x}}(\lambda) = \frac{1}{L}\left(1 - \cos\left(\frac{2\pi\lambda}{L}\right)\right)\amalg_L(\lambda). \tag{261}$$

We assume that the transmitted signal is a rectangular pulse. Thus,

$$\tilde{f}(t) = \begin{cases} \dfrac{1}{\sqrt{T}}, & 0 \le t \le T, \\ 0, & \text{elsewhere,} \end{cases}$$

$$= \frac{1}{\sqrt{T}}\amalg_T(t), \qquad -\infty < t < \infty. \tag{262}$$

We assume that the propagation time is zero for notational simplicity. (This is equivalent to redefining the time origin.) The endpoints of the observation interval are

$$T_i = 0 \tag{263}$$

and

$$T_f = T + L. \tag{264}$$

We now have the system completely specified and want to determine its performance. To evaluate $\bar{\mu}_{\text{BS}}(\frac{1}{2})$ we must evaluate $\tilde{\xi}_P(t, \tilde{s}(t), \cdot)$ for two noise levels. The function $\tilde{\xi}_P(t, \tilde{s}(t), \cdot)$ is related to $\tilde{\tilde{\xi}}(t{:}\lambda, \lambda')$ by (235).

Using (262) in (235) gives

$$\xi_P(t, \tilde{s}(t), N_0) = \frac{E_t}{T} \int_{-\infty}^{\infty} \rlap{\text{\rule[1.3ex]{0.9em}{0.4pt}}}\amalg_T(t - \lambda) \rlap{\text{\rule[1.3ex]{0.9em}{0.4pt}}}\amalg_T(t - \lambda') \tilde{\xi}(t:\lambda, \lambda')\, d\lambda\, d\lambda', \quad (265)$$

where $\tilde{\xi}(t:\lambda, \lambda')$ is specified by (227) and (228). To find $\tilde{\xi}(t:\lambda, \lambda')$, we divide it into two terms as in (229) and solve for $\tilde{p}(t:\lambda, \lambda')$. Using (254)–(257) and (261) and (262) in (230) gives

$$\frac{\partial \tilde{p}(t:\lambda, \lambda')}{\partial t} = -2k\tilde{p}(t:\lambda, \lambda') - \frac{E_t}{N_0 T}\Biggl\{ \Biggl[\frac{1 - \cos(2\pi\lambda/L)}{L}\, \rlap{\text{\rule[1.3ex]{0.9em}{0.4pt}}}\amalg_T(t - \lambda) $$

$$+ \int_{-\infty}^{\infty} \rlap{\text{\rule[1.3ex]{0.9em}{0.4pt}}}\amalg_T(t - \lambda')\tilde{p}(t:\lambda, \lambda')\, d\lambda' \Biggr] \Biggl[\frac{1 - \cos(2\pi\lambda'/L)}{L}\, \rlap{\text{\rule[1.3ex]{0.9em}{0.4pt}}}\amalg_T(t - \lambda') $$

$$+ \int_{-\infty}^{\infty} \rlap{\text{\rule[1.3ex]{0.9em}{0.4pt}}}\amalg_T(t - \lambda)\tilde{p}(t:\lambda, \lambda')\, d\lambda \Biggr]^* \Biggr\}, \quad 0 \le \lambda, \lambda' \le L, t \ge 0, \quad (266)$$

with initial conditions

$$\tilde{p}(0:\lambda, \lambda') = 0, \qquad 0 \le \lambda, \lambda' \le L. \tag{267}$$

We now demonstrate how to obtain an approximate solution to (266) by using the modal expansion technique suggested on page 501. We expand $\tilde{p}(t:\lambda, \lambda')$, using (232), as

$$\tilde{p}(t:\lambda, \lambda') = \sum_{i=1}^{\infty} \sum_{j=1}^{\infty} \tilde{p}_{ij}(t)\tilde{\phi}_i(\lambda)\tilde{\phi}_j^*(\lambda'), \qquad 0 \le \lambda, \lambda' \le L, \qquad 0 \le t \le T + L, \tag{268}$$

where the $\phi_i(\lambda)$ are an arbitrary set of orthonormal functions. Proceeding as suggested below (233), we can derive an equation specifying $\tilde{p}_{ij}(t)$. We include the details to guarantee that the actual manipulations are clear.

Modal Expansion Equations. Substituting (268) into (266) gives

$$\sum_{i=1}^{\infty} \sum_{j=1}^{\infty} \frac{\partial \tilde{p}_{ij}(t)}{\partial t}\, \tilde{\phi}_i(\lambda)\tilde{\phi}_j^*(\lambda') = -2k \sum_{i=1}^{\infty} \sum_{j=1}^{\infty} \tilde{p}_{ij}(t)\tilde{\phi}_i(\lambda)\tilde{\phi}_j^*(\lambda') $$

$$- \frac{E_t}{N_0 T}\Biggl\{ \Biggl[\Biggl(\frac{1 - \cos(2\pi\lambda/L)}{L} \Biggr) \rlap{\text{\rule[1.3ex]{0.9em}{0.4pt}}}\amalg_T(t - \lambda) $$

$$+ \int_{-\infty}^{\infty} \rlap{\text{\rule[1.3ex]{0.9em}{0.4pt}}}\amalg_T(t - \sigma) \sum_{i=1}^{\infty} \sum_{j=1}^{\infty} \tilde{p}_{ij}(t)\tilde{\phi}_i(\lambda)\tilde{\phi}_j^*(\sigma)\, d\sigma \Biggr] $$

$$\times \Biggl[\Biggl(\frac{1 - \cos(2\pi\lambda'/L)}{L} \Biggr) \rlap{\text{\rule[1.3ex]{0.9em}{0.4pt}}}\amalg_T(t - \lambda') $$

$$+ \int_{-\infty}^{\infty} \rlap{\text{\rule[1.3ex]{0.9em}{0.4pt}}}\amalg_T(t - \sigma') \sum_{i=1}^{\infty} \sum_{j=1}^{\infty} \tilde{p}_{ij}(t)\tilde{\phi}_i(\sigma')\tilde{\phi}_j^*(\lambda')\, d\sigma' \Biggr]^* \Biggr\},$$

$$0 \le \lambda, \lambda' \le L, \qquad 0 \le t \le T + L. \quad (269)$$

We now carry out the following steps:

1. Multiply both sides of (269) by $\tilde{\phi}_k^*(\lambda)\tilde{\phi}_l(\lambda')$ and integrate over λ and λ'.
2. Define

$$\tilde{z}_k(t) = \int_{-\infty}^{\infty} \left(\frac{1 - \cos{(2\pi\sigma/L)}}{L}\right)\overline{\text{III}}_T(t-\sigma)\overline{\text{III}}_L(\sigma)\tilde{\phi}_k^*(\sigma)\,d\sigma \tag{270}$$

and

$$\tilde{b}_k(t) = \int_{-\infty}^{\infty} \overline{\text{III}}_T(t-\sigma)\overline{\text{III}}_L(\sigma)\tilde{\phi}_k^*(\sigma)\,d\sigma \tag{271}$$

to simplify the equation from step 1.

3. Truncate the equation at K terms to obtain a finite-dimensional Riccati equation.

In the present problem (270) and (271) reduce to

$$\tilde{z}_k(t) = \int_a^b \left(\frac{1 - \cos{(2\pi\sigma/L)}}{L}\right)\tilde{\phi}_k^*(\sigma)\,d\sigma \tag{272}$$

and

$$\tilde{b}_k(t) = \int_a^b \phi_k^*(\sigma)\,d\sigma, \tag{273}$$

where

$$b \triangleq \min{(L, t)} \tag{274}$$

and

$$a \triangleq \min{(b, \max{(0, t - T)})}. \tag{275}$$

Carrying out the first step and using the definitions in the second step gives the differential equation

$$\frac{d\tilde{p}_{kl}(t)}{dt} = -2k\tilde{p}_{kl}(t) - \frac{E_t}{N_0 T}\,[\tilde{z}_k(t) + \sum_{j=1}^{\infty}\tilde{p}_{kj}(t)\tilde{b}_j(t)][\tilde{z}_l^*(t) + \sum_{i=1}^{\infty}\tilde{p}_{il}(t)\tilde{b}_i^*(t)]. \tag{276}$$

Truncating the series at K, we can put (276) in matrix notation as

$$\frac{d\tilde{\mathbf{p}}(t)}{dt} = -2k\tilde{\mathbf{p}}(t) - \frac{E}{N_0 T}\,[\tilde{\mathbf{z}}(t) + \tilde{\mathbf{p}}(t)\tilde{\mathbf{b}}(t)][\tilde{\mathbf{z}}(t) + \tilde{\mathbf{p}}(t)\tilde{\mathbf{b}}(t)]\dagger, \tag{277}$$

where the definition of $\tilde{\mathbf{p}}(t)$, $\tilde{\mathbf{z}}(t)$, and $\tilde{\mathbf{b}}(t)$ is clear. The initial condition is

$$\tilde{\mathbf{p}}(t) = \mathbf{0}. \tag{278}$$

We now have reduced the problem to a finite-dimensional Riccati equation, which we can solve numerically.

The final issue is the choice of the orthogonal functions $\{\tilde{\phi}_i(\lambda)\}$. We want to choose them so that the dimension of the approximating system will be small *and* so that the calculation of the quantities in (272) and (273) will be simple. As pointed out earlier, a judicious choice will reduce the computational problem significantly. In this case, the scattering function is a raised cosine function and the signal is rectangular, so that a

conventional Fourier series is a logical choice. We let

$$\tilde{\phi}_1(\lambda) = \frac{1}{\sqrt{L}} \qquad\qquad 0 \leq \lambda \leq L,$$

$$\tilde{\phi}_2(\lambda) = \sqrt{\frac{2}{L}} \cos\left(\frac{2\pi\lambda}{L}\right), \qquad 0 \leq \lambda \leq L,$$

$$\tilde{\phi}_3(\lambda) = \sqrt{\frac{2}{L}} \sin\left(\frac{2\pi\lambda}{L}\right), \qquad 0 \leq \lambda \leq L, \tag{279}$$

and so forth. We now have all of the quantities necessary to evaluate the performance.

The performance will depend on $\bar{E}_r/N_0$, k, L, and T. Before carrying out the calculations, we discuss the effect of these parameters.

First, we fix the first three parameters and study the effect of T. The length of the input signal affects the number of degrees of freedom in the output waveform. We refer to this as the system "diversity." A crude estimate of this diversity is obtained by multiplying the diversity due to Doppler spreading by the diversity due to range spreading to obtain

$$D = (1 + kT)\left(1 + \frac{L}{T}\right). \tag{280}$$

Three comments regarding (280) are useful:

1. The fading spectrum is a one-pole, and so the best bandwidth measure is not obvious; the equivalent rectangular bandwidth is $k/2$ cps (double-sided) (i.e., one might get a more accurate measure by including a constant before kT).

2. More refined diversity measures are discussed by Kennedy [37]; the expression in (280) is adequate for our intuitive discussion.

3. The expression in (280) is for a rectangular transmitted pulse and assumes that $WT = 1$.

The diversity expression in (280) is plotted as a function of $T' \triangleq T\sqrt{k/L}$ in Fig. 13.23. We see that the minimum diversity occurs when

$$T = \sqrt{\frac{L}{k}}, \tag{281}$$

and its value is

$$D_{\min} = (1 + \sqrt{kL})^2. \tag{282}$$

From our earlier work we know that there is an optimum diversity, which we would estimate as

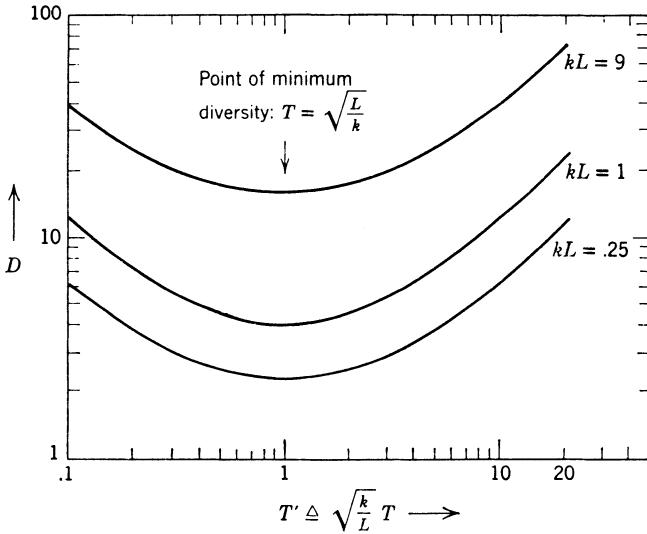$$D_{\text{opt}} \simeq \frac{1}{3} \frac{\bar{E}_r}{N_0}. \tag{283}$$

Fig. 13.23   Diversity of a doubly spread channel ($WT = 1$).

Comparing (282) and (283), we see that if

$$D_{\min} > D_{\mathrm{opt}}, \tag{284}$$

the optimum value of T will be given by (281) and the performance will decrease for either smaller or larger T, as shown in Fig. 13.24a. Intuitively, this means that the kL product is such that the channel causes more diversity than we want. On the other hand, if

$$D_{\min} < D_{\mathrm{opt}}, \tag{285}$$

the performance curve will have the general behavior shown in Fig. 13.24b. The performance will have a maximum for two different values of T.

The minimum diversity increases monotonically with the kL product, while the optimum diversity increases monotonically with $\bar{E}_r/N_0$. Therefore, for a particular kL product, we would expect the behavior in Fig. 13.24a for small $\bar{E}_r/N_0$ and the behavior in Fig. 13.24b for large $\bar{E}_r/N_0$. From our discussion in (247)–(253), we would expect that increasing the kL product will not decrease the performance significantly if $\bar{E}_r/N_0$ is large enough.

This completes our intuitive discussion. Kurth [7] has carried out the analysis for the system described in (254)–(264), using the modal expansion in (265)–(279). In Figs. 13.25 to 13.27, we show several sets of performance curves. The vertical axis is the efficiency factor,

$$\frac{\tilde{\mu}_{\mathrm{BS}}(\tfrac{1}{2})}{\bar{E}_r/N_0}.$$

$|\tilde{\mu}_{BS}(\tfrac{1}{2})|$

(*a*) Excess diversity

$|\tilde{\mu}_{BS}(\tfrac{1}{2})|$

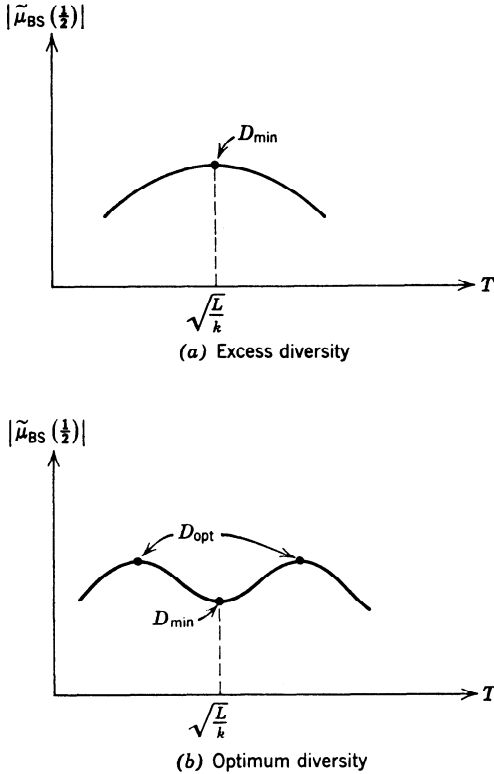(*b*) Optimum diversity

Fig. 13.24   Qualitative behavior characteristics as a function of the pulse length, *T*.

The horizontal axis is T, the pulse length. In Fig. 13.25, $kL = 0.25$, in Fig. 13.26, $kL = 1.0$, and in Fig. 13.27, $kL = 6.25$. In all cases $k = L$. The different curves correspond to various values of $\bar{E}_r/N_0$. We see that the anticipated behavior occurs. For small $\bar{E}_r/N_0$, $D_{opt} < D_{min}$, and there is a single peak. For larger $\bar{E}_r/N_0$, $D_{opt} > D_{min}$, and there are two peaks, As kL increases, a larger value of $\bar{E}_r/N_0$ is required to obtain the two-peak behavior.

In Figure 13.28, we show the effect of the kL product. To construct these curves, we used the value of T that maximized $|\tilde{\mu}_{BS}(\tfrac{1}{2})|$ for the particular kL product and $\bar{E}_r/N_0$ ($k = L$ for all curves). The vertical axis is $-\tilde{\mu}_{BS}(\tfrac{1}{2})$, and the horizontal axis is $\bar{E}_r/N_0$. Each curve corresponds to a different kL product. As the kL product increases, the exponent decreases for a fixed $\bar{E}_r/N_0$, but the change is not drastic.

This example illustrates the performance analysis of a typical system. The reader may be troubled by the seemingly abrupt transition between the
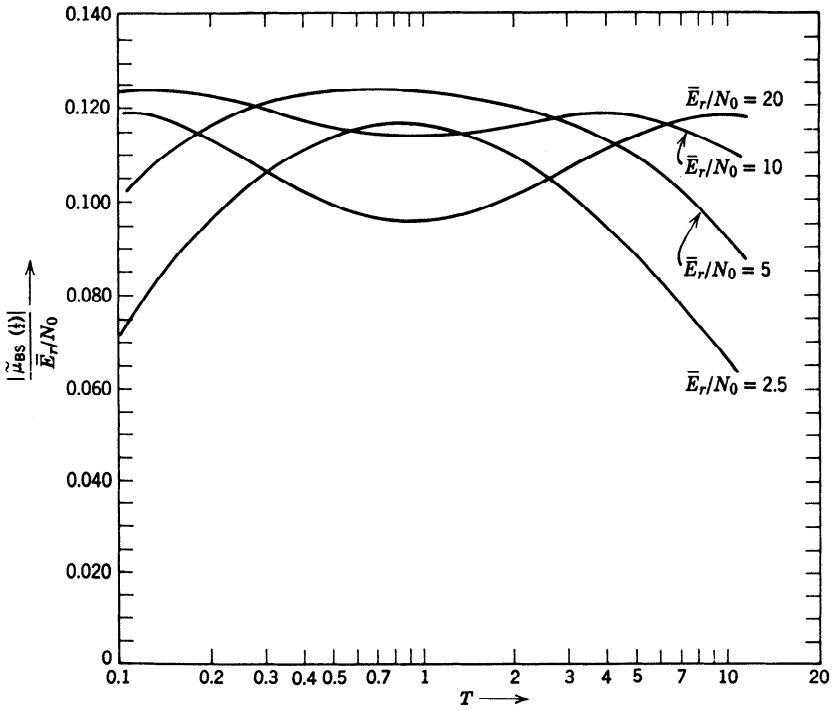
Fig. 13.25 Optimum receiver performance, binary orthogonal communication, first-order fading, underspread channel; $k = 0.5$, $L = 0.5$, constant $\tilde{f}(t)$. (From [7].)
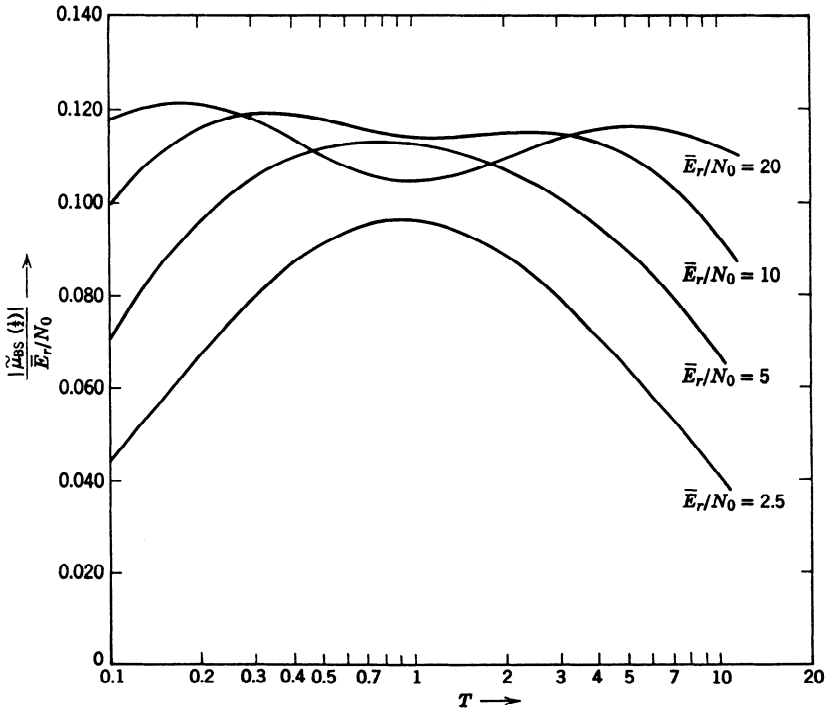

Fig 13.26 Optimum receiver performance, first-order fading, doubly-spread channel, $k = 1$, $L = 1$, constant $\tilde{f}(t)$. (From [7].)
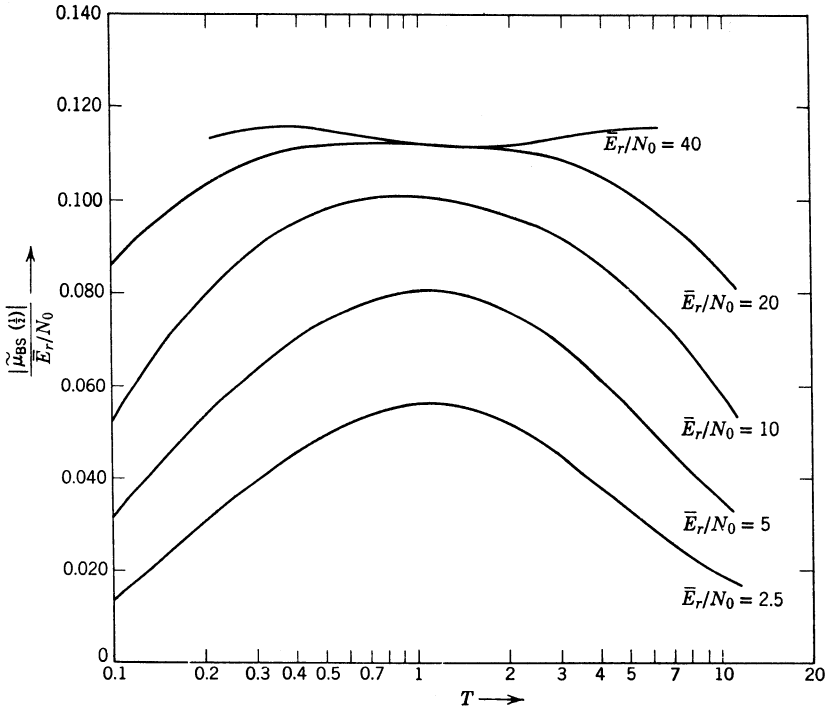
Fig. 13.27 Optimum receiver performance, binary orthogonal communication, first-order fading, overspread channel; $k = 2.5$, $L = 2.5$, constant $\tilde{f}(t)$. (From [7].)

formulas on pages 508–510 and the curves in Figs. 13.25–13.28. The intermediate steps consist of carrying out the calculations numerically. Efficient computational algorithms are important, but are not within the scope of our discussion. There is, however, one aspect of the calculation procedure that is of interest. We emphasized that a suitable choice of orthogonal functions reduces the complexity of the calculation. To generate the curves in Figs. 13.25–13.28, we kept increasing K until $\tilde{\mu}_{BS}(\tfrac{1}{2})$ stabilized. In Table 13.1, we indicate the values of K required to achieve three-place accuracy in $\tilde{\mu}_{BS}(\tfrac{1}{2})$ as a function of various parameters in the problem. When

$$W = \frac{1}{T} \ll \frac{1}{L} \tag{286}$$

or

$$T \ll \frac{1}{k} \tag{287}$$

and $\bar{E}_r/N_0$ is large, more terms are required. Notice that when (286) is satisfied we can model the channel as a Doppler-spread point channel, and
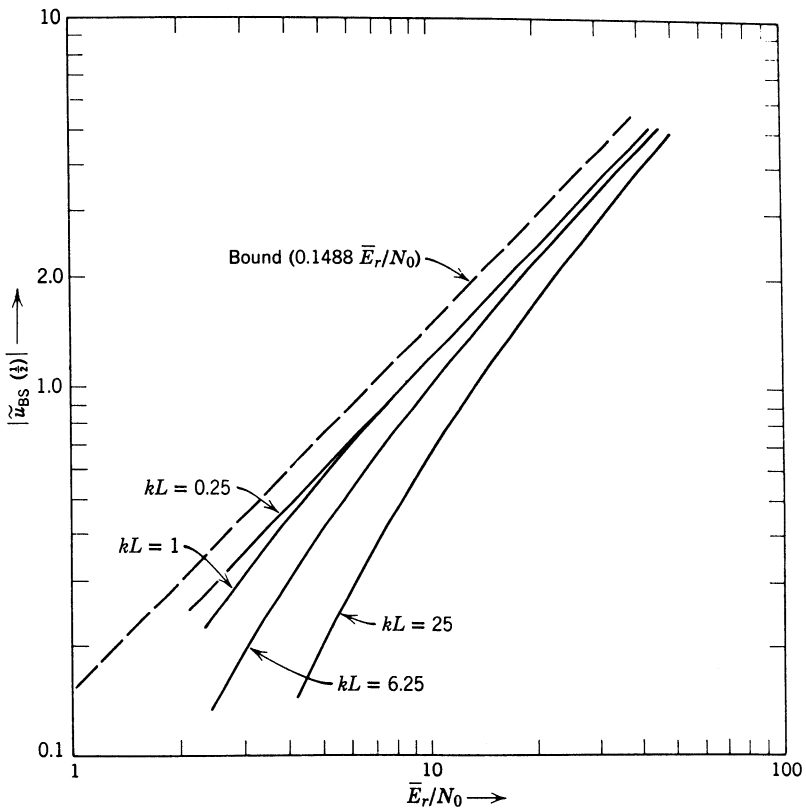
Fig. 13.28 Optimum receiver performance for optimum T, constant $\tilde{f}(t)$, binary orthogonal communication over a doubly-spread channel ($k = L$). (From [7].)

Table 13.1 Number of Terms Required to Achieve at Least Three-place Accuracy in the Calculation of $(|\tilde{\mu}_{BS}(1/2)|/\bar{E}_r/N_0)$ (From [7])

$\bar{E}_r/N_0$	k	L	T	K
5	0.5	0.5	0.1	17
5	0.5	0.5	1	13
5	0.5	0.5	10	20
20	0.5	0.5	1	13
5	1	1	1	13
5	1	1	10	21
20	1	1	1	17
5	2.5	2.5	0.1	25
5	2.5	2.5	1	17
20	2.5	2.5	1	17
20	2.5	2.5	10	25

515

when (287) is satisfied we can model the channel as a nonfluctuating range-spread channel. Thus, the cases that required the most calculation could be avoided.

In this subsection we have actually carried out the performance analysis for a specific problem. The analysis demonstrates the utility of the channel models developed in Section 13.3.2 for studying problems containing doubly-spread channels or doubly-spread targets. In addition, it demonstrates quantitatively how the various system parameters affect the system performance.

13.3.3.C.   Summary. In this section we have studied the problem of binary communication over doubly-spread channels. There are several important points that should be re-emphasized.

1. When the *BL* product of the channel is small, we can reduce it to a set of nonfluctuating point channels by proper signal design. The resulting system achieves the performance bound. Because the receiver is straightforward, this mode of operation should be used for underspread channels whenever possible.

2. When the channel is overspread, we can reduce it to a singly-spread channel by proper signal design. The efficiency of the resulting system depends on the details of the scattering function and the available $\bar{E}_r/N_0$. Because the singly-spread receiver is simpler than the doubly-spread receiver, the above mode of operation should be used for overspread channels whenever possible.

3. Most scattering functions can be adequately approximated by a distributed state-variable model. For this case, we can analyze the performance using the modal expansion techniques developed in this section. Although the analysis is complicated, it is feasible. The results provide quantitative confirmation of our intuitive arguments in simple cases and enable us to study more complicated systems in which the intuitive arguments would be difficult.

This completes our discussion of binary communication. In Section 13.3.5, we shall discuss briefly the extensions to *M*-ary systems.

13.3.4   Detection under LEC Conditions

The model for the detection problem and the binary communication problem were formulated in Section 13.3.1. In the succeeding sections we studied various facets of the general case in detail. There is one special case in which the results are appreciably simpler. This is the lower-energy-coherence (LEC) case that we have encountered several times previously.

In Section 13.3.4.A we study the LEC problem. The discussion suggests suboptimum receivers for the general case, which we discuss briefly in Section 13.3.4.B.

13.3.4.A.   LEC Receivers. If we denote the largest eigenvalue of $\tilde{s}(t)$ by $\tilde{\lambda}_{\max}$, the LEC condition is

$$\frac{\tilde{\lambda}_{\max}}{N_0} \ll 1. \tag{288}$$

Paralleling the derivation in Section 11.2.4, we can see that the likelihood ratio test for the simple binary detection problem reduces to

$$l_R = \frac{1}{N_0^2} \iint\limits_{T_i}^{T_f} \tilde{r}^*(t) \tilde{K}_{\tilde{s}}(t, u) \tilde{r}(u) \, dt \, du \underset{H_0}{\overset{H_1}{\gtrless}} \gamma. \tag{289}$$

Substituting (143) into (289) gives

$$l_R = \frac{E_t}{N_0^2} \iint\limits_{T_i}^{T_f} dt \, du \int_{-\infty}^{\infty} d\lambda \, \tilde{r}^*(t) \tilde{f}(t - \lambda) \tilde{K}_{DR}(t - u, \lambda) \tilde{f}^*(u - \lambda) \tilde{r}(u) \underset{H_0}{\overset{H_1}{\gtrless}} \gamma. \tag{290}$$

A particularly simple realization can be obtained when $T_i = -\infty$ and $T_f = \infty$ by factoring $\tilde{K}_{DR}(t - u, \lambda)$ along the time axis as

$$\tilde{K}_{DR}(t - u, \lambda) = \int_{-\infty}^{\infty} \tilde{K}_{DR}^{[\frac{1}{2}]*}(z - t, \lambda) \tilde{K}_{DR}^{[\frac{1}{2}]}(z - u, \lambda) \, dz. \tag{291}$$

Using (291) in (290) gives

$$l_R = \frac{E_t}{N_0^2} \int_{-\infty}^{\infty} dz \int_{-\infty}^{\infty} d\lambda \left| \int_{-\infty}^{\infty} \tilde{K}_{DR}^{[\frac{1}{2}]}(z - u, \lambda) \tilde{f}^*(u - \lambda) \tilde{r}(u) \, du \right|^2. \tag{292}$$

The receiver specified by (292) is shown in Fig. 13.29 (due originally to Price [5]). Because the receiver requires a continuous operation in λ, it cannot be realized exactly. An approximation to the optimum receiver is obtained by sampling in λ and replacing the λ integration by a finite sum. This realization is shown in Fig. 13.30. This receiver is also due to Price [5] and is essentially optimum under LEC conditions.

When the LEC condition is valid, (11.65) gives

$$\tilde{\mu}(s) \simeq - \frac{s(1 - s)}{2N_0^2} \iint\limits_{T_i}^{T_f} |\tilde{K}_{\tilde{s}}(t, u)|^2 \, dt \, du. \tag{293}$$

Using (143) in (293) gives

$$\tilde{\mu}(s) \simeq - \frac{s(1 - s)}{2}$$

$$\times \left\{ \frac{E_t^2}{2N_0^2} \iint\limits_{-\infty}^{\infty} dt \, du \int_{-\infty}^{\infty} d\lambda_1 \tilde{f}(t - \lambda_1) \tilde{K}_{DR}(t - u, \lambda_1) \tilde{f}^*(u - \lambda_1) \right.$$

$$\left. \times \int_{-\infty}^{\infty} d\lambda_2 \tilde{f}^*(t - \lambda_2) \tilde{K}_{DR}^*(t - u, \lambda_2) \tilde{f}(u - \lambda_2) \right\}. \tag{294}$$
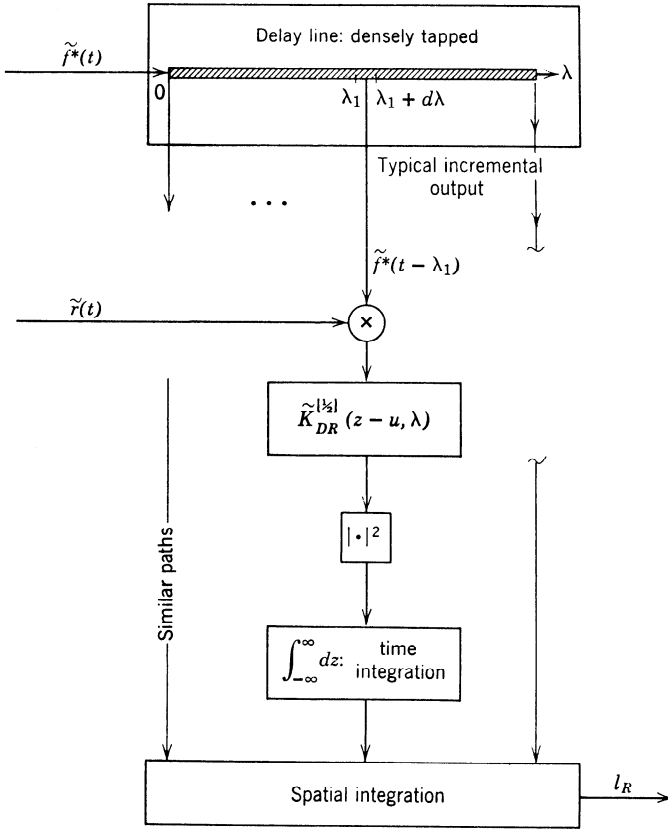
Fig. 13.29   Optimum LEC receiver for doubly-spread channel.

This can be written more compactly as

$$\tilde{\mu}(s) = -\frac{s(1-s)}{2}\left\{\frac{E_t^2}{N_0^2}\iint\limits_{-\infty}^{\infty}\theta\{\tau, v\}\,|\tilde{R}_{DR}\{\tau, v\}|^2\,d\tau\,dv\right\}, \qquad (295)$$

where $\theta\{\tau, v\}$ is the signal ambiguity function, and $\tilde{R}_{DR}\{\tau, v\}$ is the two-frequency correlation function defined in (21). (See Problem 13.3.21)

Our discussion of the LEC problem has been brief, but the reader should not underestimate its importance. In many cases the system is forced to operate under LEC conditions. Then the results in (292) and (295) are directly applicable. In other cases the LEC condition is not present, but the LEC receiver suggests a suboptimum receiver structure. We explore this problem briefly in the next subsection.
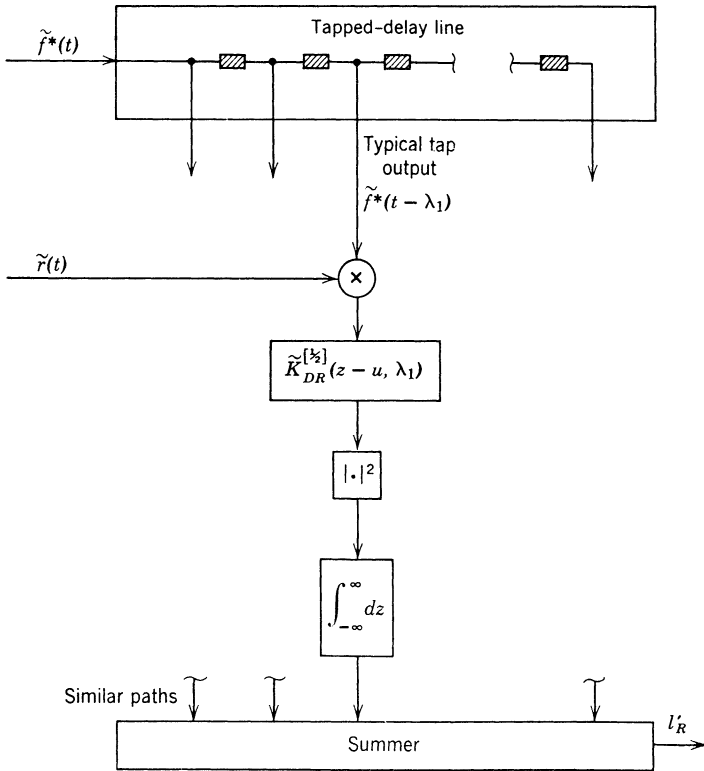
Fig. 13.30 Approximation to optimum LEC receiver for doubly-spread channel.

13.3.4.B. Suboptimum Receivers. The first suboptimum receiver follows directly from Fig. 13.30. We retain the structure but allow an arbitrary time-invariant filter in each path. Thus,

$$l_{so} = \sum_{i=1}^{K} \int_{-\infty}^{\infty} dz \left| \int_{-\infty}^{\infty} \tilde{h}(z - u, \lambda_i) \tilde{f}^*(u - \lambda_i) \tilde{r}(u) \, du \right|^2. \qquad (296)$$

The performance of this receiver can be analyzed by combining the techniques of Sections 11.3 and 13.3.3. By varying the $\tilde{h}(\cdot, \lambda_i)$, we can optimize the performance within the structural limitations. The actual calculations are complicated but feasible.

The second suboptimum receiver is a generalization of the receivers in Figs. 11.19 and 12.11. This receiver is shown in Fig. 13.31. Notice that there are N_R branches and each branch contains N_D correlation operations.